Structure-Activity Relationship Analysis of Inhibitors Targeting an Insect Steroid Hormone Biosynthesis Regulator Noppera-bo

January 2021

Kazue INABA

Structure-Activity Relationship Analysis of Inhibitors Targeting an Insect Steroid Hormone Biosynthesis Regulator Noppera-bo

A dissertation Submitted to
the Graduate School of Life and Environmental Sciences, the
University of Tsukuba
in Partial Fulfillment of the Requirements
for the Degree of Doctor of Philosophy in Science
(Doctoral Program in Biological Sciences)

Kazue INABA

Structure-Activity Relationship Analysis of Inhibitors Targeting an Insect Steroid Hormone Biosynthesis Regulator Noppera-bo

A dissertation Submitted to
the Graduate School of Life and Environmental Sciences,
the University of Tsukuba
in Partial Fulfillment of the Requirements
for the Degree of Doctor of Philosophy in Science
(Doctoral Program in Biological Sciences)

Kazue INABA

Table of contents

Abbreviations

20E: 20-hydroxy ecdysone
7HI: 7-hydroxyisoflavone
AeNobo: *Aedes aegypti* Nobo
BioA: Biochanin A
DTT: 1,1,1-trichloro-2,2-bis-(p-chlorophenyl)ethane
DZN: Daidzein
DmNobo: *Drosophila melanogaster* Nobo
ERα: Estrogen receptor alpha
ERβ: Estrogen receptor alpha
EST: 17β-Estradiol
EcR : Ecdysone receptor
FMO: The fragment molecular orbital
FOR: Formononetin
G-site: Glutathione binding site
GEN: Genistein
GSH: Glutathione
GST: Glutathione *S*-transferase
GSTD: Glutathione *S*-transferase delta
GSTE: Glutathione *S*-transferase epsilon
H-site: Hydrophobic site
IGR: Insect growth regulator
MD: Molecular dynamics
Nobo : Noppera-bo
SA: simulated annealing
SAR: structure-activity relationship analysis
THI: 4′, 6, 7-trihydroxyisoflavone
hGSTP1-1: Human GST pi 1-1

Chapter 1

An integrated approach unravels a crucial structural property for the function of the insect steroidogenic Halloween protein Noppera-bo

Abstract

Ecdysteroids are the principal insect steroid hormones essential for insect development and physiology. In the last 18 years, several enzymes responsible for ecdysteroid biosynthesis, encoded by Halloween genes, have been identified and well characterized, both genetically and biochemically. However, none of these proteins have yet been characterized at the tertiary structure level. Here, I report an integrated in silico, *in vitro*, and *in vivo* analyses of the Halloween glutathione S-transferase (GST) protein, Noppera-bo (Nobo). I determine crystal structures of *Drosophila melanogaster*. Nobo (DmNobo) complexed with glutathione and 17β-estradiol, a DmNobo inhibitor. 17β-estradiol almost fully occupied the putative ligand-binding pocket, and a prominent hydrogen bond formed between Asp113 of DmNobo and 17β-estradiol. Asp113 is essential for inhibiting DmNobo enzymatic activity by 17β-estradiol, as 17β-estradiol does not inhibit and physically interacts less with the Asp113Ala DmNobo point mutant. Asp113 is highly conserved among Nobo proteins, but not among other GSTs, implying that Asp113 is important for endogenous Nobo function. Indeed, a homozygous nobo allele possessing the Asp113Ala point mutation exhibits embryonic lethality with undifferentiated cuticle structure, a phenocopy of complete loss-of-function nobo homozygotes. These results suggest that the nobo family of GST proteins has acquired a unique amino acid residue, which seems to be essential for binding an endogenous sterol substrate to regulate ecdysteroid biosynthesis. This is the first study to reveal the structural characteristics of insect steroidogenic Halloween proteins. This study also provides basic insight into applied entomology for developing a new type of insecticides that specifically inhibit ecdysteroid biosynthesis.

Introduction

Ecdysteroids play pivotal roles in regulating many aspects of development and physiology in arthropods, including insects (Niwa and Niwa 2014; Yamanaka, Rewitz, and O'Connor 2012). Because ecdysteroids do not exist naturally in animals other than arthropods, it has been long thought that molecules involved in ecdysteroid biosynthesis, secretion, circulation and reception could be good targets for developing third-generation pesticides that specifically inhibit insect life cycles, with no adverse effects on other animals (Williams 1967). Thus, the study of ecdysteroids has been important, not only in the basic biological sciences, but also in the field of applied agrobiology.

Ecdysteroids are biosynthesized from dietary sterols that are primarily obtained from food sources (Niwa and Niwa 2014; Yamanaka et al. 2012). The formation of each biosynthetic intermediate going from dietary sterols such as cholesterol to the biologically-active form of ecdysteroids, 20-hydroxyecdysone (20E), is catalyzed by a specific ecdysteroidogenic enzyme (Gilbert 2004; Niwa and Niwa 2014). Since 2000, a series of these enzymes has been identified. These enzymes include Neverland (Yoshiyama-Yanagawa et al. 2011; Yoshiyama 2006), Non-molting glossy/Shroud (Niwa et al. 2010), Spook/CYP307A1 (Namiki et al. 2005; Ono et al. 2006), Spookier/CYP307A2 (Ono et al. 2006), CYP6T3 (Ou, Magico, and King-Jones 2011), Phantom/CYP306A1 (Niwa et al. 2004; Warren et al. 2004), Disembodied/CYP302A1 (Warren et al. 2002), Shadow/CYP315A1 (Warren et al. 2002), and Shade/CYP314A1 (Petryk et al. 2003). A deficiency of genes encoding these enzymes results in developmental lethality. Particularly, in the fruit fly *Drosophila melanogaster,* complete loss-of-function mutants of *shroud*, *spook*, *phantom*, *disembodied*, *shade*, and *shadow*, which are often classified as Halloween mutants, commonly result in embryonic lethality with the loss of differentiated cuticle structures (Chavez et al. 2000). To date, the functions of these enzymes have been characterized genetically and some of them have also been analyzed biochemically (Niwa and Niwa 2014; Saito et al. 2016). However, none of these enzymes have yet been characterized at the tertiary structure level.

Here, I report the first crystal structure of an ecdysteroidogenic regulator encoded by the Halloween gene, *noppera-bo* (*nobo*) (Chanut-Delalande et al.

2014; Enya et al. 2014, 2015). *nobo* encodes a member of the epsilon class of cytosolic glutathione *S*-transferases (GST, EC 2.5.1.18; hereafter GSTEs) (Saisawang, Wongsantichon, and Ketterman 2012). In general, GSTs catalyze various reactions with an activated glutathione (GSH) molecule in the following 3 ways: GSH conjugation to a substrate, reduction of a substrate using GSH, and isomerization (Wu and Dong 2012). Data from previous studies have demonstrated that *nobo* is specifically expressed in ecdysteroidogenic tissues, including the prothoracic gland and the adult ovary (Chanut-Delalande et al. 2014; Enya et al. 2014, 2015). Loss-of-*nobo*-function mutations in *D. melanogaster* and *Bombyx mori* result in developmental lethality, which are well rescued by administering 20E (Chanut-Delalande et al. 2014; Enya et al. 2014, 2015). In addition, the *D. melanogaster* mutants are also rescued by cholesterol, which is the most upstream compound in the ecdysteroid biosynthesis pathway (Enya et al. 2014). Consistent with the requirement of GSH for GST function, a defect in glutathione biosynthesis in *D. melanogaster* also leads to larval lethality, which is partly rescued by the administration of 20E or cholesterol (Enya et al. 2017). These data indicate that the *nobo* family of GSTs is essential for ecdysteroid biosynthesis by regulating cholesterol trafficking and/or metabolism. However, besides GSH, an endogenous ligand and a catalytic reaction driven by Nobo have not been elucidated.

In this study, I utilized the vertebrate female sex hormone 17β-estradiol (EST, Fig. 1-1A) as a molecular probe to gain insight into Nobo ligand recognition, based on our previous finding that EST inhibits the GSH-conjugation activity of *D. melanogaster* Nobo (DmNobo; also known as DmGSTE14) (Fujikawa et al. 2015). I therefore considered the complex of DmNobo and EST to be an ideal target for elucidating a 3-dimensional structure of an ecdysteroidogenic Halloween protein and characterizing the interaction between DmNobo and its potent inhibitor. Moreover, I used an integrated, combined approach based on quantum chemical calculations, molecular dynamics (MD) simulations, biochemical and biophysical analyses, and molecular genetics. Consequently, I identified one DmNobo amino acid residue that is strongly conserved only in the Nobo family of GSTs, which is crucial for DmNobo inhibition by EST and for the normal *in vivo* function of DmNobo during *D. melanogaster* embryogenesis.

Results

Crystal structure of DmNobo

The crystal structure of the apo-form of DmNobo (DmNobo_Apo) was determined at 1.50 Å resolution by the molecular replacement method (Table 1-1). DmNobo forms a polypeptide homodimer with a canonical GST fold, which has a well-conserved GSH-binding site (G-site) and a hydrophobic substrate-binding pocket (H-site) adjacent to the G-site (Mashiyama et al. 2014; Wu and Dong 2012). The crystal structures of the DmNobo_GSH, DmNobo_EST, and DmNobo_EST-GSH complexes were also determined at resolutions of 1.75 Å, 1.70 Å, and 1.55 Å, respectively (Fig. 1-1B, Table 1-1). The crystal structures of the DmNobo_EST and DmNobo_EST-GSH complexes reproducibly showed clear electron densities for EST. GSH and EST binding did not affect the overall structure of DmNobo; the root-mean-square deviation (RMSD) values for each pair among the four crystal structures were comparable with respect to the estimated coordinate errors (Table 1-2).

GSH, a common substrate of GSTs (Mashiyama et al. 2014; Wu and Dong 2012), was found in the G-site of DmNobo. Crystallographic analysis revealed that the position and conformation of GSH in DmNobo, and interaction between GSH and DmNobo were essentially identical to those in other GSTEs (Low et al. 2010; Riveron et al. 2014; Scian et al. 2015). GSH is recognized by an intensive hydrogen bond network with Gln43, His55, Val57, Pro58, Asp69, Ser70, His71, and Ser107 in the G-site (Fig. 1-2A). Moreover, these residues are well conserved among not only GSTEs but also the delta and theta classes of GSTs (hereafter GSTD proteins and GSTT proteins, respectively), which are closely related to GSTEs (Fig. 1-2B) (Saisawang et al. 2012). Therefore, I conclude that the interaction between the G-site and GSH cannot account for the unique functional property of DmNobo, as compared to other GSTD/E/T proteins.

Molecular mechanism of EST recognition by DmNobo

EST was bound in the H-site, which has a hydrophobic character. The electron-density map clearly showed that the compound in the H-site was the intact EST molecule (Fig. 1-1C). The EST molecule had no chemical modifications, including reduction and *S*-glutathionylation. The H-site, of which volume is

approximately 365 Å^3, was mostly filled with the EST molecule, which has a volume of approximately 350 Å^3, and no space was available to accommodate another compound in the H-site (Fig. 1-3A-3C).

Of the 16 amino acid residues lining the H-site, Arg13, Ser14, Gln43, Arg122, and Met212 do not have direct contacts with EST (Table 1-3). The D-ring of EST is situated near the entrance of the H-site and exposed to the solvent. Only a few interactions are observed between the D-ring of EST and DmNobo (Fig. 1-4A, Table 1-3). In contrast, the A-ring of EST is located deep inside of the H-site and makes intensive hydrophobic interactions with H-site residues (Pro15, Leu38, Phe39, Phe110, Ser114, Met117, and Leu208) (Fig. 1-4A, Table 1-3). Another amino acid residues interact with other portions of EST, such as Ser118 at the side of C-ring, Val121 near C18, and Thr172 near O3. These amino acid residues interacting with EST are well conserved among the Nobo proteins but not among DmGSTD/E/T proteins (Fig. 1-5A-5F, Table 1-3). These results suggest that the three-dimensional structure of the H-site, particularly near the A-ring of EST, is conserved in Nobo proteins and has different characteristics from DmGSTD/E/T proteins.

While the H-site has an overall hydrophobic character, there is one charged residue, Asp113, in the H-site. Asp113, which is nearly completely conserved in the Nobo proteins (see below), is located at the innermost region of the H-site. EST binding induces a rotation of the $\chi 1$ angle of Asp113 by 25.4°, and Oδ of Asp113 forms a hydrogen bond with O3 of EST (Fig. 1-4B). This is the only hydrogen bond found between EST and DmNobo and seems to be critical for EST binding.

To evaluate the contribution of the hydrogen bond to the interaction with EST, total interaction energies between EST fragments and DmNobo amino acid residues were calculated using the fragment molecular orbital (FMO) method, which can evaluate the inter-fragment interaction energy (IFIE) based on the quantum chemistry (Fedorov and Kitaura 2007; Tsukamoto et al. 2015). The FMO calculation classifies the IFIE into 4 energy categories, namely the electrostatic energy (ES), exchange-repulsion energy (EX), charge-transfer energy and higher-order mixed term (CT+mix), and dispersion energy (DI). The FMO calculation estimated that the ES represented approximately half of the total IFIE (-41.4 kcal/mol versus -82.4 kcal/mol; Fig. 2C). The crystal structure suggested that the ES arises from the hydrogen bond between Oδ of Asp113

and O3 of EST (Table 1-4). These results suggested that Asp113 plays a critical role in interacting with EST.

Asp113 in DmNobo is essential for EST binding

The importance of the Asp113-EST hydrogen bond for EST binding was biochemically examined with a recombinant mutated DmNobo protein carrying Asp113Ala amino acid substitution (DmNobo[Asp113Ala]). DmNobo[Asp113Ala] lacks the sidechain carboxyl group at position 113 and therefore cannot form a hydrogen bond with EST. The crystal structure of the DmNobo[Asp113Ala] did not show significant structural differences compared with the wild-type DmNobo (DmNobo[WT]) protein .

I first examined the enzymatic activities of DmNobo[WT] and DmNobo[Asp113Ala] using an *in vitro* enzymatic assay system with the fluorogenic substrate 3,4-DNADCF (Fujikawa et al. 2015). In this assay system, GSTs catalyze GSH conjugation to the non-fluorescent molecule, 3,4-DNADCF, giving rise to highly fluorescent product, 4-GS-3-NADCF. In the absence of EST, both DmNobo[WT] and DmNobo[Asp113Ala] showed GSH-conjugation activity (Fig. 1-6C) although the activity of DmNobo[Asp113Ala] decreased by approximately half of DmNobo[WT]. In the presence of EST, as expected from the EST-binding to the H-site, the enzymatic activity of DmNobo[WT] was inhibited with an IC_{50} value of approximately 2.3 μM (Fig. 1-6A, C). In contrast, the enzymatic activity of DmNobo[Asp113Ala] was not inhibited by EST, even at a concentration of 25 μM (Fig. 1-6A, C).

I next measured the dissociation constant (*K*d) values between DmNobo and EST by performing surface plasmon-resonance (SPR) analysis. The *K*d values between DmNobo[WT] and EST in the presence or absence of GSH were 0.38 ± 0.02 μM and 0.48 ± 0.10 μM, respectively (Fig. 1-6B, Fig. 1-6C). In contrast, it was barely possible to determine the *K*d value between DmNobo[Asp113Ala] and EST due to a weak interaction (Fig. 1-6B, Fig. 1-6C), which was consistent with crystal structure analysis. These results suggest that Asp113 is critical for interaction with EST.

I also employed MD simulations to confirm the contribution of Asp113 to the interaction with EST using DmNobo[WT] and DmNobo[Asp113Ala] as models. In these MD simulations, the initial structures of EST and the DmNobo proteins were defined based on data acquired from the crystallographic analyses (Fig.

4D). While simulating DmNobo[WT] for 100 nano seconds (ns), I found that the distance between Oγ of Asp113 and the hydroxyl group of EST was relatively constant (Fig. 1-6E and 1-6F). However, when simulating DmNobo[Asp113Ala], the distance between Ala113 and the hydroxyl group of EST increased over time, and EST moved from the initial position (Fig. 1-6E and 1-6F). Among three independent MD simulations, the maximum RMSD value of EST in DmNobo[WT] was less than ~6.60 Å. In contrast, with the MD simulation of DmNobo[Asp113Ala], the maximum RMSD value was less than ~9.54 Å. These simulation results also support the possibility that hydrogen bonding between Asp113 and EST is required for stable binding of EST to the H-site.

Evolutionary conservation of Asp113 in Noppera-bo

The *nobo* family of GSTs is well conserved in Diptera and Lepidoptera (Ayres et al. 2011; Enya et al. 2014; Yu et al. 2008). Amino acid-sequence analysis revealed that all Nobo proteins from 6 dipteran and 13 lepidopteran species have Asp at the position corresponding to Asp113 of DmNobo (Fig. 1-5A, Fig. 1-5B, Fig. 1-5D). An exception is found in Nobo of the yellow fever mosquito *Aedes aegypti*, as the corresponding amino acid residue of *A. aegypti* Nobo is Glu, which also has a carboxyl group in the sidechain similar to Asp. In contrast, no Asp/Glu residue was found at the corresponding position of the DmGSTD/E/T proteins, other than Nobo (Fig. 1-5C, Fig. 1-5E, Fig. 1-5F). Consistent with the amino acid composition, EST inhibited the enzymatic activity of the African malaria mosquito *Anopheles gambiae* Nobo (AgNobo), but not that of the DmGSTE6 or DmGSTE9 recombinant proteins (Fig. 1-5G). Furthermore, as well as DmNobo[Asp113Ala], a point mutation of AgNobo at Asp111 to Ala attenuated inhibitory activity of EST against its enzymatic activity (Fig. 1-7). These results suggest that Nobo proteins utilize Asp113 to recognize their target compounds as a common feature and that Asp113 serves a biological role.

Asp113 is essential for *Drosophila melanogaster* embryogenesis

Finally, I examined whether Asp113 is essential for any *in vivo* biological function of DmNobo. I utilized a CRISPR-Cas9-based knock-in strategy to generate a *nobo* allele encoding an Asp113Ala point mutation ($nobo^{3\times FLAG\text{-}HA\text{-}D113A}$). I found that no trans-heterozygous mutant *D. melanogaster* with

nobo$^{3\times FLAG\text{-}HA\text{-}D113A}$ and the complete loss-of-*nobo*-function allele (*nobo*^{KO}) (Enya et al. 2014) survived to the adult stage (Table 1-4). By performing a detailed developmental-stage analysis, we identified no first-instar larvae or later-staged insects with the *nobo*$^{3\times FLAG\text{-}HA\text{-}D113A}$/*nobo*^{KO} genotype. These results indicate that the *nobo*$^{3\times FLAG\text{-}HA\text{-}D113A}$/*nobo*^{KO} genotype is embryonic lethal. I also found that *nobo*$^{3\times FLAG\text{-}HA\text{-}D113A}$/*nobo*^{KO} embryos exhibit an undifferentiated cuticle phenotype (Fig. 1-8A, Fig. 1-8B) and a failure of head involution (Fig. 1-8C, Fig. 1-8D). These phenotypic characteristics were very similar to the feature of Halloween mutants, such as *nobo*^{KO}/*nobo*^{KO} homozygotes (Enya et al. 2014). We confirmed that the protein level of Nobo$^{3\times FLAG\text{-}HA\text{-}D113A}$ was comparable to that of Nobo$^{3\times FLAG\text{-}HA\text{-}WT}$ (Fig. 1-8E, Fig. 1-8F), suggesting that the phenotypes were due to loss of protein function, but not impaired gene expression. Taken together, these results show that Asp113 of DmNobo serves a biological function in normal development from the embryonic stage to the adult stage.

Discussion

In this study, I employed an integrated experimental approach, involving *in silico, in vitro*, and *in vivo* analyses to unravel the structure–function relationship of the ecdysteroidogenic GST protein, Nobo. GSTs are widely expressed in all eukaryotes and are also massively duplicated and diversified (Mashiyama et al. 2014). Among them, the Nobo family of GST proteins is strictly required for ecdysteroid biosynthesis in insects. Importantly, the lethality of *nobo* mutation in *D. melanogaster* is rescued by overexpressing *nobo* orthologues, but not by overexpressing non-*nobo*-type *gst* genes involved in detoxification and pigment synthesis (Enya et al. 2014). This fact strongly indicates that, when compared to canonical GSTs, Nobo proteins must possess a unique structural property that make Nobo specialized for ecdysteroid biosynthesis. Regarding this point, this study is significant in that I found that the unique acidic amino acid, Asp/Glu113, is crucial for the *in vivo* function of Nobo. It should be noted that, besides Asp/Glu113, other amino acids constituting the H-sites are also highly conserved among 21 Nobo proteins (Fig. 1-5A, Fig. 1-5B, Fig. 1-5D). These common features imply that the Nobo proteins might share an identical endogenous ligand for the H-site in the ecdysteroidogenic tissues among the species.

An endogenous ligand for Nobo remains a mystery. This study, however, provides some clues for considering candidates for an endogenous ligand. First, it is very likely that the ligand forms a hydrogen bond with the Oδ/Oγ atom of Asp/Glu113, given that the *nobo* Asp113Ala point mutation was embryonic lethal and the complete loss-of-function *nobo* phenocopy in mutant *D. melangaster*. Second, considering the complementary shape between the H-site and EST, it seems reasonable to predict that the endogenous ligand(s) is at least similar in shape to steroids. This prediction is also supported by the fact that Nobo acts in ecdysteroidogenic tissues where steroidal molecules are enriched. One steroid that possesses these features is cholesterol. Evidence from our previous study suggests that *nobo* may be involved in cholesterol transport and/or metabolism in ecdysteroidogenic tissues (Chanut-Delalande et al. 2014; Enya et al. 2014, 2015). Very interestingly, an MD simulation indeed predicted that cholesterol can stably bind to the H-site of DmNobo via a hydrogen bond between the hydroxyl group of cholesterol (C3 position) and

Asp113 of DmNobo (Fig. 1-9). However, paradoxically, it seems that cholesterol contains no site for a chemical reaction with GSH by DmNobo. It is possible that Nobo might serve as a carrier or a transporter for the ligand in cells, possibly cholesterol, as several classes of GSTs have been shown to exhibit "ligandin" function (Simons and Vander Jagt 1980), which might be an initial step of the ecdysteroid biosynthesis pathway. Currently, I have failed in multiple attempts to detect DmNobo-cholesterol complexes via crystallographic analyses, and further experiments are needed for clarify any interaction between Nobo and cholesterol.

The activities of insect ecdysteroids can be disrupted *in vivo* using chemical agonists and antagonists of the ecdysone receptor, some of which are also utilized as insecticides (Nakagawa and Henrich 2009). However, chemical compounds that specifically inhibit ecdysteroid biosynthesis are not available. This study provides the first structural information for guiding the development of efficient Nobo inhibitors, which might serve as seed compounds for new insecticides in the future. However, it should be noted that EST and estrogenic chemical compounds are often recognized as dangerous endocrine-disrupting chemicals against wild animals (Pinto, Estêvão, and Power 2014). Therefore, while EST is a prominent inhibitor of Nobo, a practical compound that can be utilized as an actual insecticide must display no-estrogenic activity. To consider this problem, it is important to note a difference in the EST-recognition patterns between DmNobo and the mammalian estrogen receptor alpha (ERα) protein (Avvakumov et al. 2002; Brzozowski et al. 1997; Pedersen et al. 2002; Pike et al. 1999). The details of the EST-ERα interaction were investigated using the crystal structures of human ERα in an EST-bound form (Brzozowski et al. 1997; Fukuzawa et al. 2006). In ERα, Glu353 interacts with the O3 atom of EST, Phe404 interacts with the A-ring of EST via a CH/π interaction, His524 interacts with the O17 atom of EST, and hydrophobic residues interact with the steroid nucleus. Each of these recognition patterns were found in DmNobo such as a hydrogen bond between Asp113 and O3 atom of EST and an SH/π interaction between Cys residue of GSH and the A-ring of EST, except for a hydrogen bond with the O17 atom of EST (Fig. 1-10). Given this difference, I expect that a Nobo-specific, non-estrogenic chemical compound can be developed. Currently, I'm pursuing large-scale computational calculations to

select chemical compounds that satisfy those conditions and an *in vitro* enzymatic assay to examine DmNobo inhibition.

I emphasize that this report is the first to describe the physical interactions between a Halloween protein and a potent inhibitor at the atomic level. Our interdisciplinary approach will also be applicable for Nobo proteins other than *D. melanogaster*, such as disease vector mosquitos and the agricultural pest moths, and might be a viable strategy for developing new insecticides useful for human societies.

Figures and tables

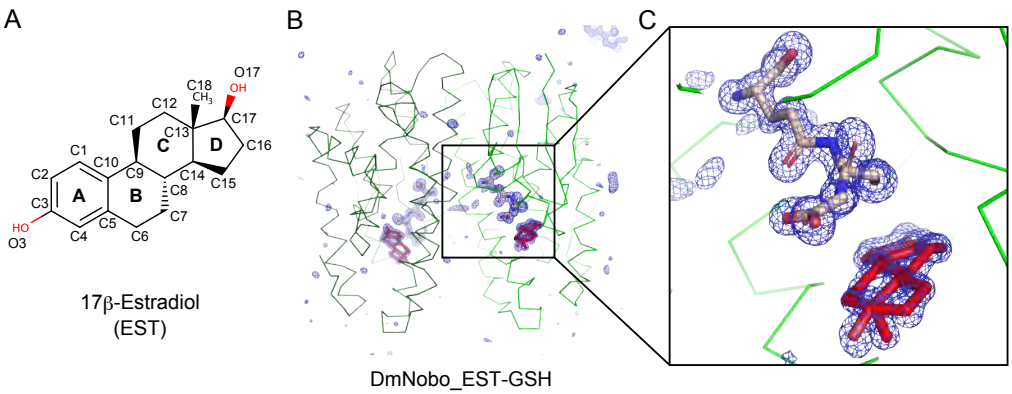

Figure 1-1. Crystal structures of the *Drosophila melanogaster* Noppera-bo protein

(A) Chemical structure of 17β-estradiol (EST). The atoms of the steroid nucleus are indicated. Rings A, B, C, and D are also shown. (B) Simulated annealing-omit map for GSH and EST in the DmNobo_EST-GSH complex. A mFo-DFc map (blue) (4.0 Å within 5.0 Å from the protein atoms is shown. Carbon atoms of DmNobo, GSH, and EST are colored green, wheat, and red, respectively. Oxygen and nitrogen atoms are colored green and blue, respectively. (C) An enlarged view of (B) around the EST and GSH ligands

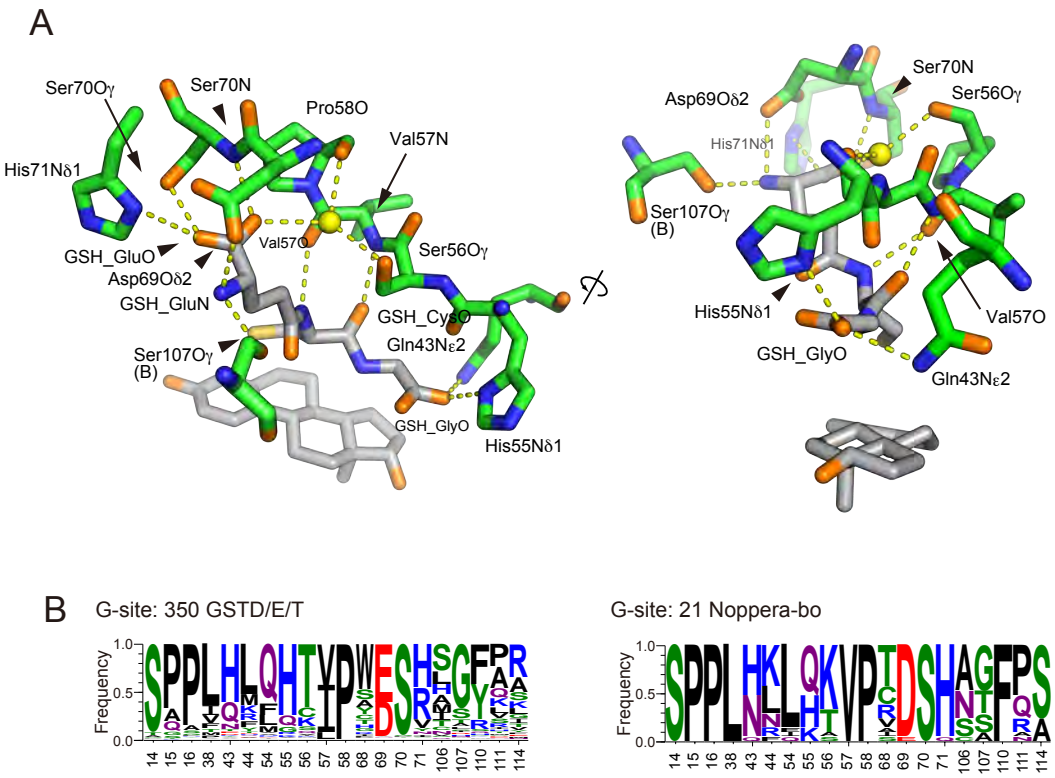

Figure 1-2. Glutathione binding site (G-site) of DmNobo

(A) A hydrogen-bond network between DmNobo and GSH. Hydrogen bonds are indicated with yellow dashed lines. Carbon atoms of the protein and ligands (GSH, EST) are shown in green and gray, respectively. One of the two conformations of Ser107, in which the Oγ atom is directed towards GSH, is shown. (B) Frequencies of amino acid residues composing the G-site of 350 GSTD/E/T (left) and 21 Nobo (right) proteins displayed in A. The frequencies were calculated using LOGO, and Nobo proteins were excluded from the GSTD/E/T proteins for the frequency calculation.

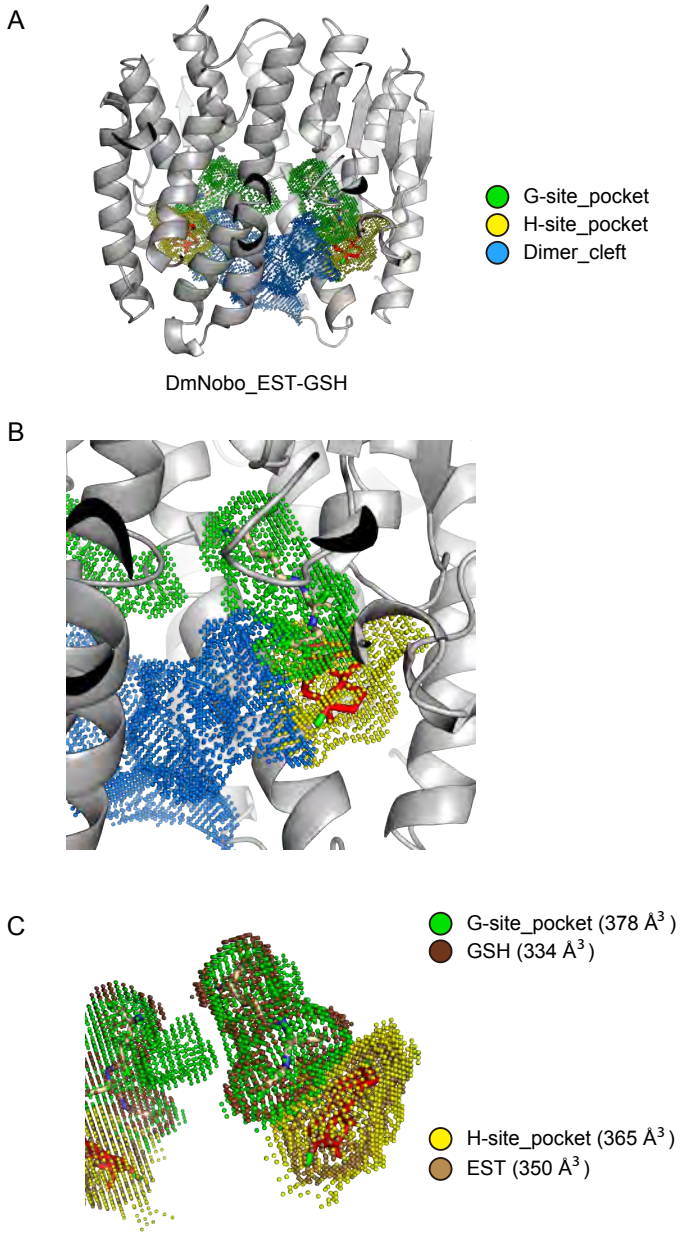

Figure 1-3. Pockets in the G- and H-sites of DmNobo

(A, B) Pockets in DmNobo were calculated using 3V. The inner surfaces of the two pockets, i.e., the G- and H-sites, are represented in green and yellow dots, respectively. The cleft between the two subunits of the DmNobo_EST-GSH are shown in blue. The G-site was calculated using the crystal structure of the DmNobo_EST-GSH complex without GSH, and the H-site was calculated using the crystal structure of the DmNobo_EST-GSH complex without EST. (B) An enlarged view of the G- and H-sites. (C) The solvent-accessible surfaces of GSH

and EST are represented with brown and light brown dots, respectively. The surfaces of the G- and H-sites are superimposed on GSH (green) and EST (yellow).

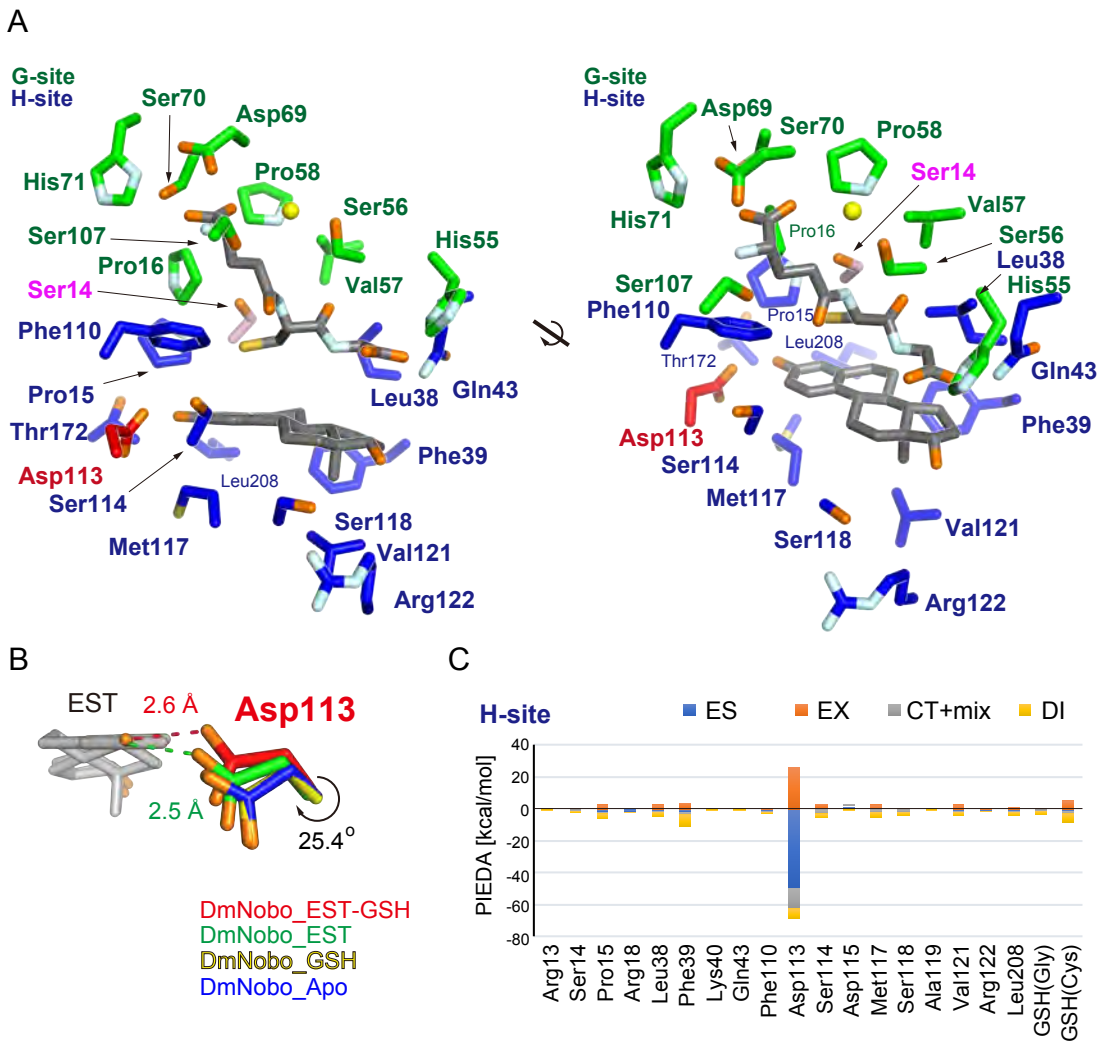

Figure 1-4. Asp113 in the H-site interacts with 17β-estradiol.

(A) GSH- and EST-interacting residues. Carbon atoms of the G- and H-sites are colored in green and blue, respectively. Common residues of the G- and H-sites (Ser14, Pro15, Leu38, Gln43, and Phe110) are assigned as those of the H-site in this figure. Carbon atoms in Ser14, Asp113, and ligands (GSH and EST) are colored in pink, red, and gray, respectively. A water molecule interacting with each ligand is represented with a yellow sphere. (B) Conformational change of Asp113 upon ligand binding. Carbon atoms in DmNobo_Apo, DmNobo_GSH, DmNobo_EST, and DmNobo_EST-GSH are shown in blue, yellow, green, and red, respectively. A hydrogen bond between the O3 atom of EST and Oγ in Asp113 is indicated by a dashed line. The difference in the χ1 torsion angle of Asp113 between DmNobo_GSH and DmNobo_EST-GSH was

25.4°. (C) Interaction energies between EST and other atoms in the DmNobo_EST-GSH complex. The interaction energies were calculated from the PIEDA analysis, based on the FMO calculation. ES, EX, CT+mix, and DI indicate the electrostatic energy, exchange repulsion energy, charge transfer energy and higher order mixed term, and dispersion energy, respectively. Residues within a distance of twice the van der Waals radii from the EST atoms are shown. Numerical data for (C) are available in Table 1-4.

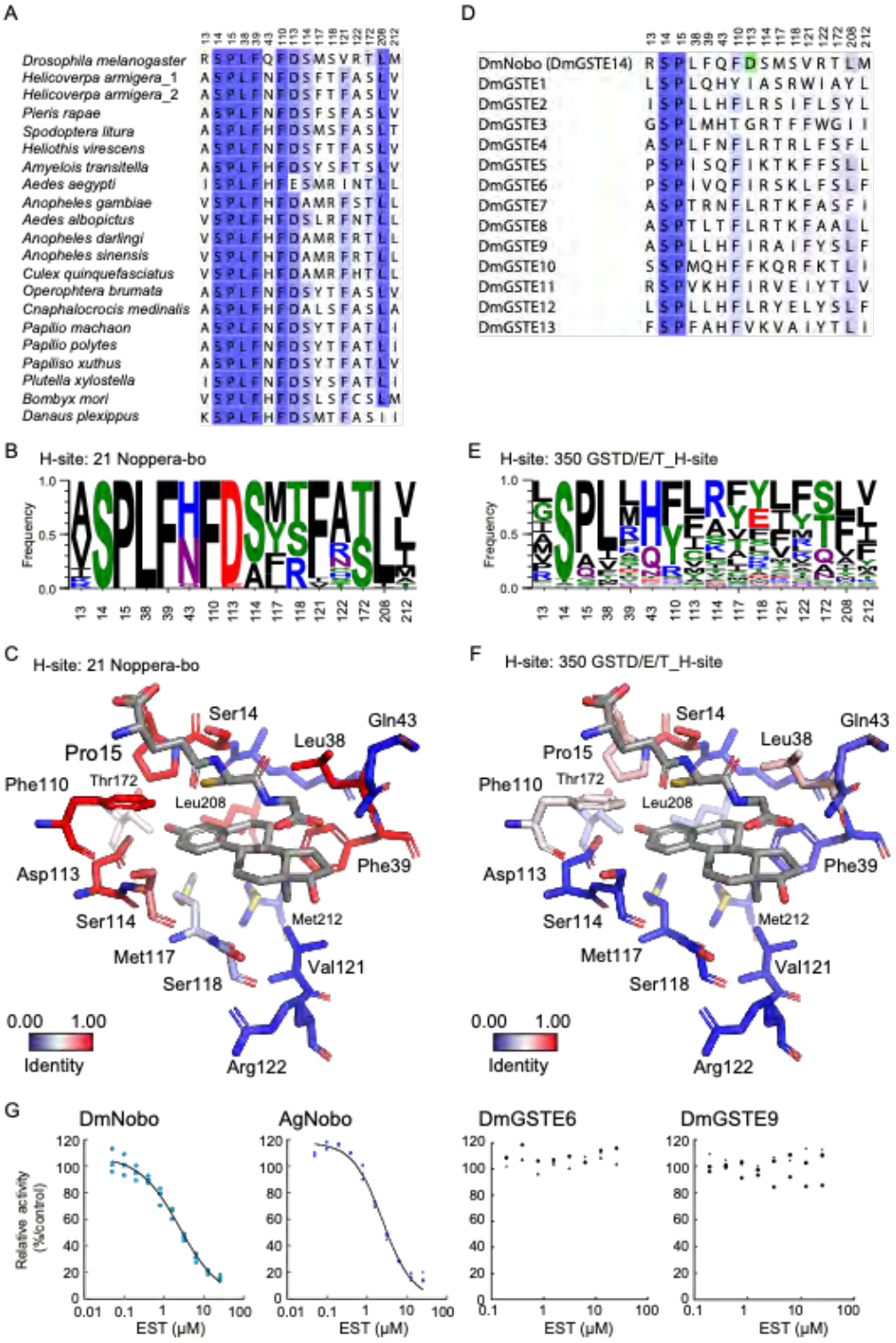

Figure 1-5. Consensus amino acid residues in the H-sites of Nobo orthologues

(A) Amino acid-sequence alignment of the H-site residues of 21 Nobo orthologues. These sequences were aligned using COBALT and manually edited, based on the crystal structure of DmNobo. The accession numbers of Helicoverpa armigera_1 and _2 are XP_021192638.1 and A0A2W1BRE1, respectively. (B) Frequencies of amino acid residues forming the H-sites of 21 Nobo. The frequencies were calculated using LOGO. (C) Conservation ratios of H-site residues among Nobo proteins are mapped to the tertiary structure of DmNobo. (D) Amino acid-sequence alignment of the H-site residues of DmGSTE. Asp113 of DmNobo is colored in green. (E) Frequencies of amino acid residues forming the H-sites of GSTD/E/T proteins. The frequencies were calculated using LOGO. (F) Conservation ratios of H-site residues among GSTD/E/T proteins including Nobo proteins (Table 1-2) are mapped to the tertiary structure of DmNobo. (G) EST-dependent inhibition of the GSH-conjugation activities of DmNobo, AgNobo, DmGSTE6, and DmGSTE9. 3,4-DNADCF was used as an artificial fluorescent substrate. Each relative activity is defined as the ratio of activity, when compared to the respective proteins without EST. All of the data points in triplicate assays are indicated. The values of IC_{50} were 2.33 (± 0.08) μM for DmNobo, 2.07 (± 0.36) μM for AgNobo, >25 μM for DmGSTE6 and >25 μM for DmGSTE9.

A

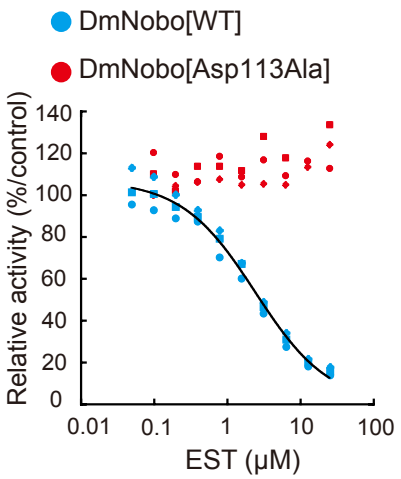

B

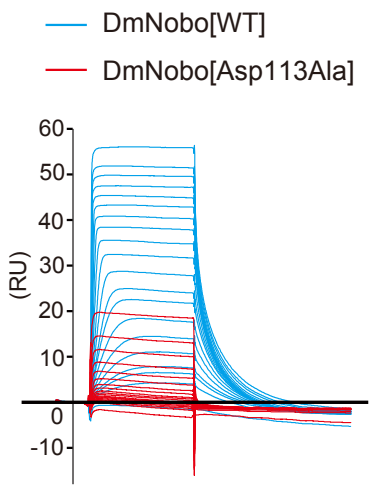

C

	Catalytic activity* (μmol/min/mg-protein)	IC50 of EST† (μM)	*Kd* against EST +/- GSH (μM)
DmNobo [WT]	2.60 (± 0.31)‡	2.33 (± 0.08)	0.38 (± 0.02) / 0.48 (± 0.10)
DmNobo [Asp113Ala]	1.01 (± 0.02)	> 25.0	incalculable / incalculable

D

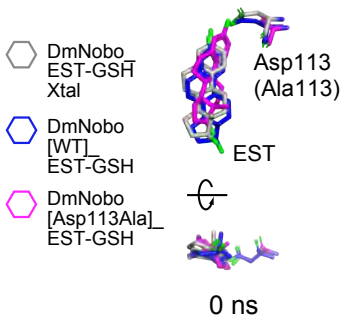

E

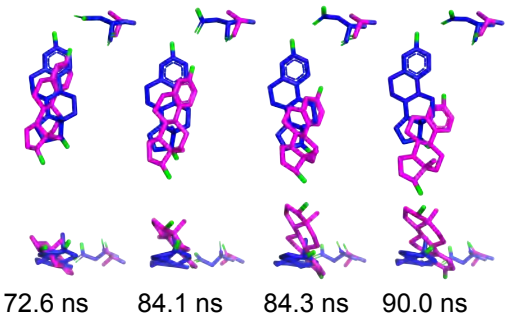

F

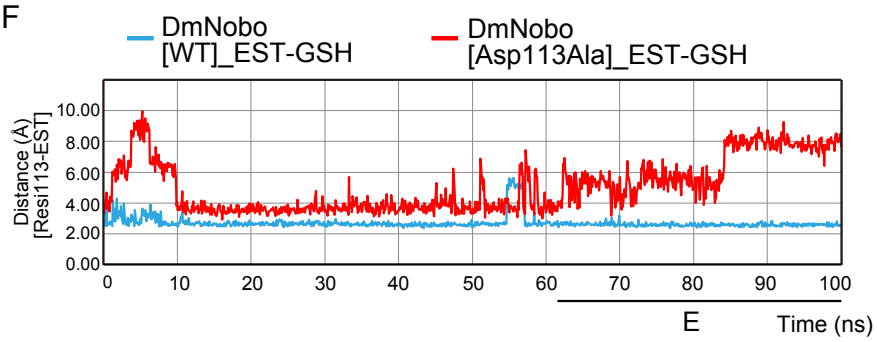

Figure 1-6. Asp113 is essential for DmNobo binding to EST.

(A) EST-dependent inhibition of the GSH-conjugation activity of DmNobo[WT] (cyan) and DmNobo[Asp113Ala] (red). 3,4-DNADCF was used as an artificial fluorescent substrate. In each case, the relative activity is defined as the ratio of activity, when compared to DmNobo[WT] without EST. All of the data points in triplicate assays are shown. (B) Sensorgrams of surface plasmon-resonance analysis of DmNobo proteins with EST. DmNobo[WT] or DmNobo[Asp113Ala] was immobilized to a sensor chip, and solutions containing a series of EST concentrations were applied in presence of 1 mM GSH. (C) Kinetic parameters of DmNobo proteins. Catalytic activity (*) and IC_{50} of EST (†) indicate 3,4-DNADCF-specific GSH-conjugation activity and the IC_{50} of EST against 3,4-DNADCF-specific GSH-conjugation activity, respectively. Values in parentheses indicate standard deviation from triplicate assays (‡). (D–F) *In silico* evaluation of the contribution of Asp113 to the interaction between DmNobo and EST. MD simulations of the DmNobo[WT] or DmNobo[Asp113Ala] complex with EST and GSH in a TIP3P-water model were carried out at 300 K for 100 ns. These simulations were performed in triplicate. (D) MD models at 0 ns of DmNobo with EST and GSH (blue), DmNobo[Aps113Ala] with EST and GSH (magenta), and the crystal structure of DmNobo_EST-GSH (EST-GSH_Xtal, gray). The upper models are shown from above the EST ligand, and the lower models are rotated 90° from the upper models. Hydrogen atoms are not shown. (E) MD models of DmNobo[WT]_EST-GSH and DmNobo[Asp113Ala]_EST-GSH from 72.6 ns to 90.0 ns. (F) Distance between Oγ of Asp113 of DmNobo[WT] or Cγ of DmNobo[Asp113Ala] and the O3 atom of EST at each frame.

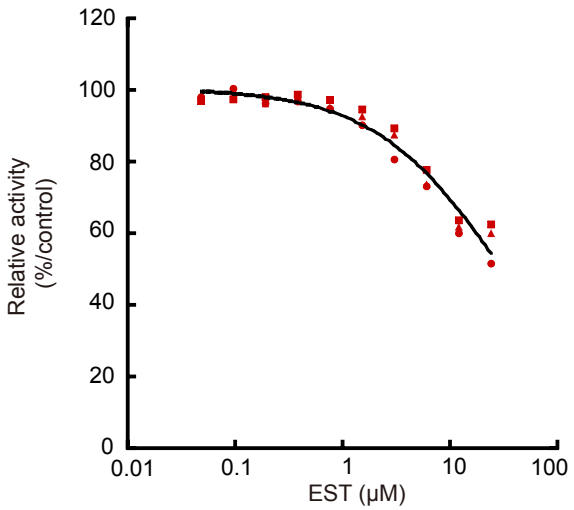

Figure 1-7. EST-dependent inhibition of the GSH-conjugation activities of AgNobo[Asp111Ala].

3,4-DNADCF was used as an artificial fluorescent substrate. Relative activity is defined as the ratio of activity, when compared to the protein without EST. All of the data points in triplicate assays are indicated. The IC_{50} value was >25 μM.

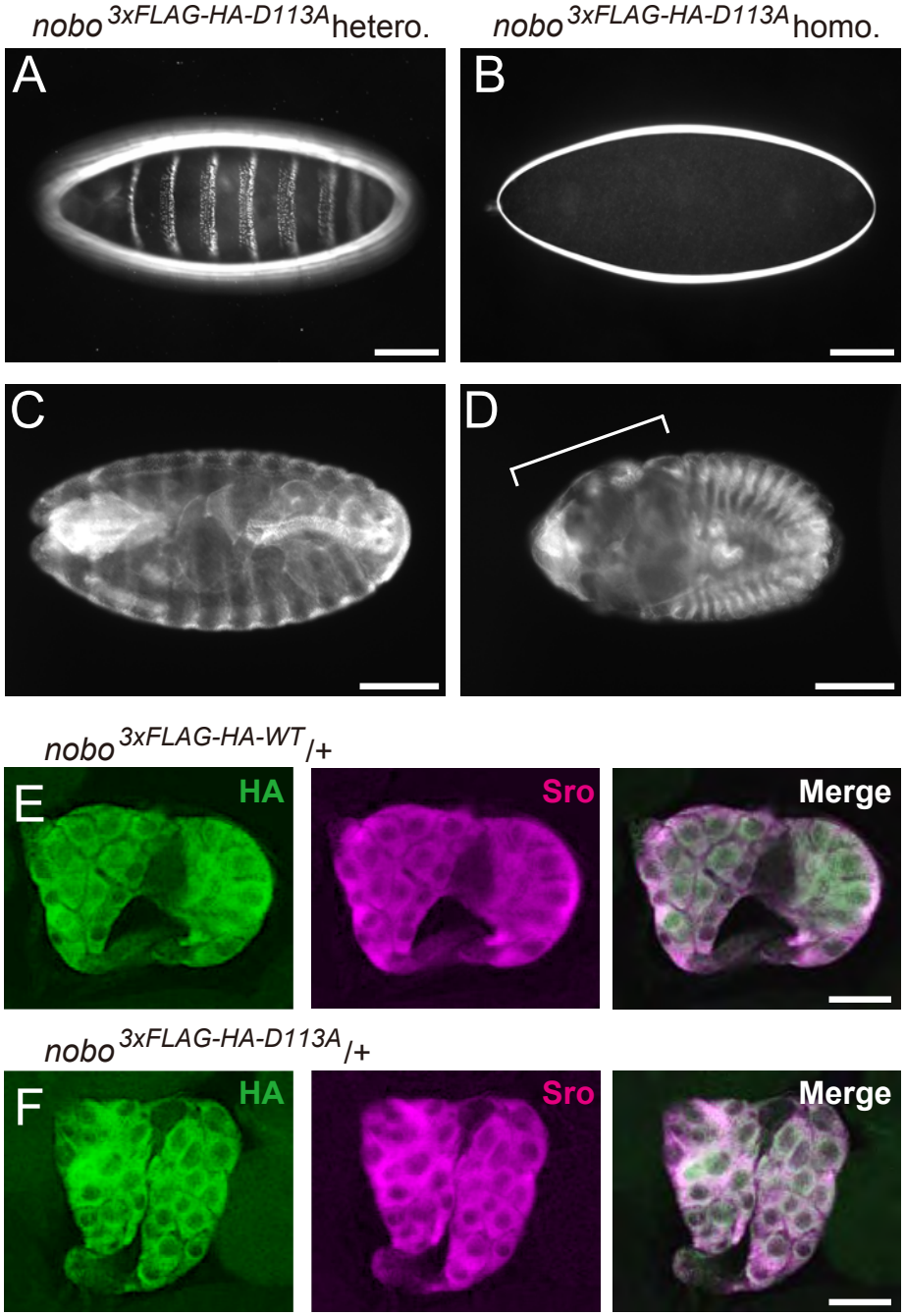

Figure 1-8. ***in vivo*** **analyses of Asp113Ala**

(A, B) Dark-field images of embryonic cuticles from *nobo*$^{3\times FLAG\text{-}HA\text{-}D113A}$ heterozygotes (*nobo*$^{3\times FLAG\text{-}HA\text{-}D113A}$/CyO; A) and homozygotes (*nobo*$^{3\times FLAG\text{-}HA\text{-}D113A}$/*nobo*$^{3\times FLAG\text{-}HA\text{-}D113A}$; B)

(C, D) Anti-FasIII antibody staining to visualize overall embryo morphologies. (C) nobo3$^{\times FLAG\text{-}HA\text{-}D113A}$ heterozygotes. (D) *nobo*$^{3\times FLAG\text{-}HA\text{-}D113A}$ homozygotes. The bracket indicates defective head involution.

(E, F) Immunohistochemistry for the ring glands from nobo$^{3\times FLAG\text{-}HA\text{-}D113}$-heterozygous (E) and *nobo*$^{3\times FLAG\text{-}HA\text{-}D113A}$-heterozygous (F) third-instar larvae. Green and magenta represent the immunostaining observed with anti-HA and anti-Shroud (Sro) antibodies, respectively. Sro was detected as a marker of the prothoracic gland. Scale bars: 100 μm for A–D and 50 μm for E and F.

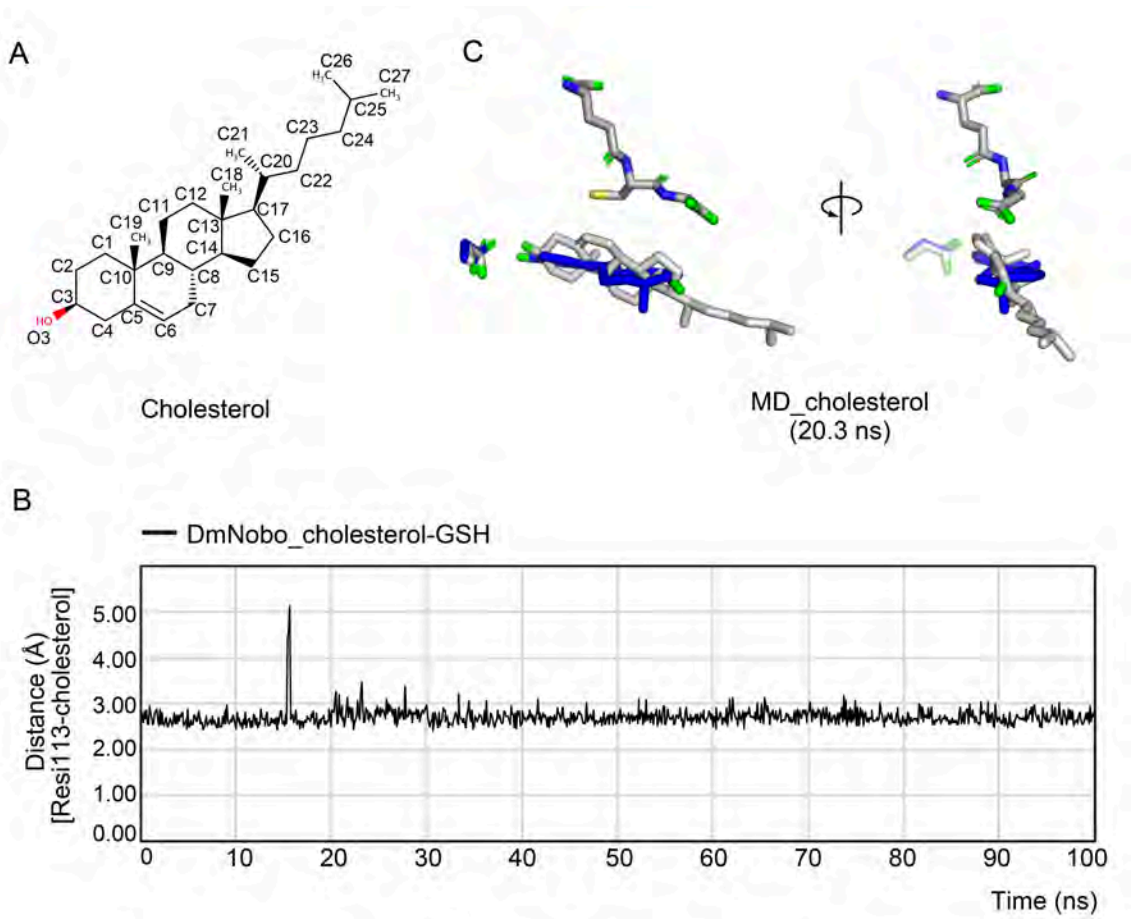

Figure 1-9. *In silico* evaluation of interaction between DmNobo and cholesterol

(A) Chemical structure of cholesterol. (B) MD-simulation results for DmNobo in complex with cholesterol and GSH. The distance between Oγ of Asp113 of DmNobo and O3 of cholesterol was plotted against time. (C) MD models of DmNobo_cholesterol-GSH and DmNobo_EST-GSH at 20.3 ns.

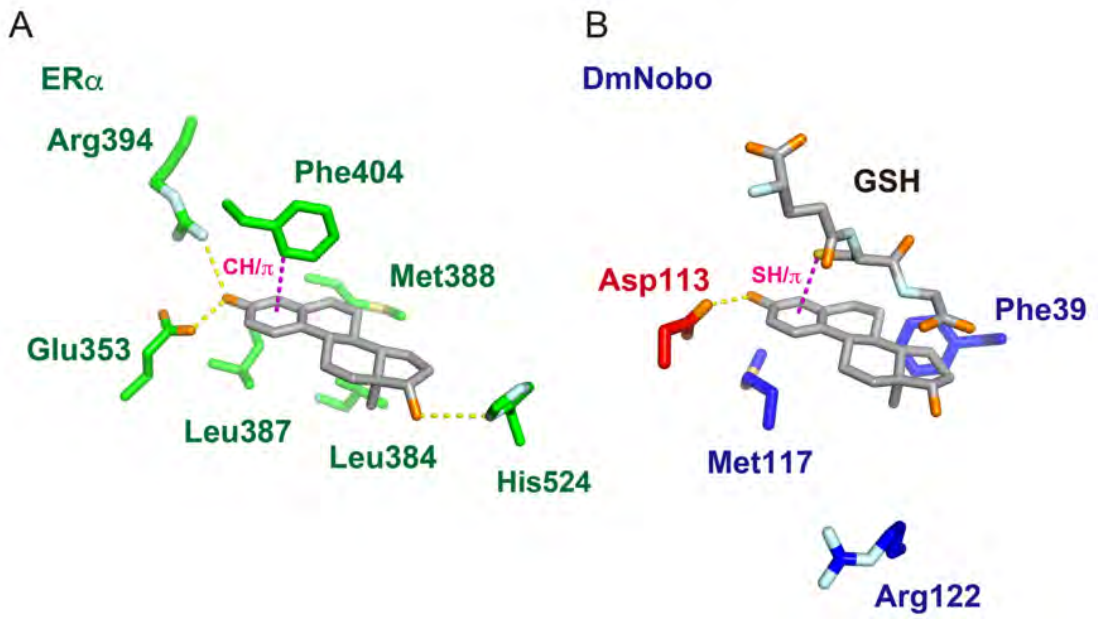

Figure 1-10. Comparison of the DmNobo_EST and ERα_EST interactions.
Side chains of representative residues of ERα (A) or DmNobo (B) that interact with EST are represented with sticks (PDB ID for ERα structure = 1QKT). A hydrogen bond between the protein and EST is indicated with a yellow dashed line. A CH/π interaction between Phe404 and EST or an SH/π interaction between GSH and EST is indicated with a pink dashed line.

Table1-1. Crystallographic Summary of DmNobo crystal structures

	DmNobo_Apo	DmNobo _GSH	DmNobo_EST	DmNobo _EST-GSH
Data Collection				
Space group	$P2_12_12_1$	$P2_12_12_1$	$P2_12_12_1$	$P2_12_12_1$
Cell Dimensions				
a, *b*, *c* (Å)	59.12, 76.56 106.36	58.75, 75.67, 107.84	58.40, 75.08, 109.02	58.38, 75.06, 108.52
α, β, γ (°)	90.00, 90.00, 90.00	90.00, 90.00, 90.00	90.00, 90.00, 90.00	90.00, 90.00, 90.00
Resolution* (Å)	42.83 - 1.50 (1.55 - 1.50)	46.42 - 1.75 (1.81 - 1.75)	46.12 - 1.58 (1.64 - 1.58)	46.11 - 1.55 (1.61 - 1.55)
R_{merge}	0.045 (0.38)	0.082 (1.05)	0.048 (0.84)	0.038 (0.36)
I/σI	33.8 (6.53)	27.3 (2.3)	37.6 (2.6)	42.7 (3.3)
Completeness	1.00 (1.00)	1.00 (0.97)	0.87 (0.47)	0.95 (0.69)
Redundancy	13.1 (12.7)	14.3 (12.2)	14.1 (10.6)	12.3 (3.8)
CC1/2	1.00 (0.97)	1.00 (0.75)	1.00 (0.76)	1.00 (0.84)
Refinement				
Resolution (Å)	42.83 - 1.50	35.70 - 1.75	35.49 - 1.70	32.59 - 1.55
No. of reflections	77,842	49,095	51,170	65,906
R_{work}	0.164	0.173	0.176	0.161
R_{free}	0.195	0.207	0.211	0.182
No. of Atoms				
Protein	3,880	3,609	3,687	3,817
GSH	0	40	0	40
EST	0	0	40	40
Water	643	408	403	499
B factors				
Protein	22.0	22.0	23.5	20.1
GSH	-	17.7	-	15.5
EST	-	-	31.5	20.8
Waters	39.5	33.7	34.5	34.7
RMSD				
Bond length (Å)	0.008	0.007	0.008	0.010
Bond angles (°)	0.98	0.89	0.96	1.19
Ramachandran prot (%)				
favored	99.1	99.3	98.9	99.3
allowed	0.90	0.68	1.14	0.68
outliers	0.00	0.00	0.00	0.00
PDB ID	6KEM	6KEN	6KEO	6KEP

Each structure was determined from diffraction data from one crystal. PDB, Protein Data Bank; RMSD, root-mean-square deviation. *Highest resolution shells are shown in parentheses.

Table 1-2. root-mean-square deviation (RMSD) among DmNobo crystal structures

		RMSD (Å) of Cα atoms of chain A†/ RMSD (Å) of Cα atoms of chains A and B‡		
	Coordinate error (Å)*	DmNobo_GSH	DmNobo_EST	DmNobo_EST-GSH
DmNobo_Apo	0.13	0.20 / 0.35	0.26 / 0.42	0.48 / 0.55
DmNobo_GSH	0.20		0.16 / 0.24	0.42 / 0.36
DmNobo_EST	0.21			0.40 / 0.32
DmNobo_EST-GSH	0.15			

* Coordinate errors are estimated by a maximum-likelihood method.

† Number of aligned Cα atoms in chain A: 199 atoms

‡ Number of aligned Cα atoms in chain A and B: 391 atoms

Table 1-3. Summary of H-site-composing, or EST-interacting atoms in DmNobo

* Atoms of DmNobo within 4.0 Å from EST. † Atoms of EST within 4.0 Å from each EST-interacting atom. ‡ Average of chains A and B in the asymmetric unit.

Residue	H-site-composing atoms	EST-interacting atoms*	DmNobo-interacting atoms†	Distance ‡ (Å)	Identity among DmGST D/E/T	Identity among Nobo	Total IFIE to EST (kcal/mol)
Arg13	C, Cβ	-	-	-	0.07	0.05	-0.31
Ser14	Cα, N, Cβ	-	-	-	0.85	1.00	-1.78
Pro15	Cδ, C	Cδ	O3	3.2	0.62	1.00	-3.93
		Cδ	C3	3.6			
		Cδ	C4	3.7			
		Cγ	O3	3.1			
Leu38	C, O, Cβ, Cδ	Cβ	C15	4.0	0.61	1.00	-1.86
		Cδ	C7	4.0			
Phe39	Cα, Cδ, Cγ, Cε, Cζ	Cε1	C6	3.9	0.07	1.00	-6.77
			C7	3.7			
		π	C15	3.9			
Gln43	Nε	-	-	-	0.21	0.05	-0.51
Phe110	Cε, Cζ	Cε	C2	4.0	0.42	1.00	-2.79
Asp113	Oδ	Oδ	O3	2.6	0.01	0.95	-41.4
Ser114	Cα, Cβ	Cα	C1	3.8	0.10	0.76	-2.17
		Cα	C2	3.8			
		Cβ	C1	3.9			
Met117	Cβ, Cγ, Cε	Cβ	C1	3.9	0.04	0.40	-3.52
		Cβ	C2	3.9			
		Cγ	C2	3.8			
		Cγ	C3	3.9			
Ser118	Cα, N, Cβ, Cγ	-	-	-	0.06	0.33	-3.25
Val121	Cβ, Cγ1, Cγ2	Cβ	C18	3.9	0.11	0.05	-1.63
		Cγ1	C18	3.9			
		Cγ2	C18	3.8			
Arg122	Cβ	-	-	-	0.07	0.14	-1.49
Thr172	Cγ	Cγ	O3	3.3	0.31	0.52	0.026
Leu208	Cδ1, Cδ2	Cδ1	C4	3.9	0.31	0.95	-2.17
		Cδ1	C6	3.8			
		Cδ2	O3	4.0			
		Cδ2	C4	3.9			
Met212	Sδ	-	-	-	0.05	0.95	-0.65
GSH	Cys_Cβ, Cys_Sγ	Cys_Sγ	π	3.7	-	-	-3.48

Table 1-4. Viability of *nobo*$^{3\times\text{FLAG-HA-D113A}}$/*nobo*^{KO} knock-in animals

Background	Knock-in gene	Mating *w*; *nobo*^{KO}/ CyO-GFP (female) ×	Number of adults Cy- (Cy+)*	Number of first instar larvae without GFP (with GFP)
nobo^{KO}	*nobo*$^{3\times FLAG\text{-}HA\text{-}WT}$	*w*; *nobo*$^{3\times FLAG\text{-}HA\text{-}WT}$/ CyO-GFP (male)	83 (172)	N.D. †
	nobo$^{3\times FLAG\text{-}HA\text{-}D113A}$	*w*; *nobo*$^{3\times FLAG\text{-}HA\text{-}D113A}$/ CyO-GFP (male)	0 (187)	0 (157)

* Cy- and Cy+ indicate animals with straight wings and curly wings, respectively.
† N.D. indicates "not determined".

Materials and Methods

Protein expression and purification

The protein-expression plasmid pCold-III (Takara Bio Inc., Kusatsu, Japan) was used to express recombinant GST proteins in *E. coli*. Coding sequences (CDSs) of *Drosophila melanogaster nobo* (*CG4688, Dmnobo*), *gste6* (*CG17530, Dmgste6*), *gste9* (*CG17534, Dmgste9*), and *Anopheles gambiae gste8* (*AGAP009190*, *Agnobo*) were amplified by the polymerase chain reaction (PCR) using complementary DNA derived from *D. melanogaster* larvae. The primers used for PCR were nobo-Fwd (5′-CAGTCATATGATGTCTCAGCCCAAGCCGATTTTG-3′), nobo-Rev (5′-CTCGAGCTACTCCACCTTCTCGGTGACTACCG-3′), GSTe6-Fwd (5′-CATATGATGGTGAAATTGACTTTATACGG-3′), GSTe6-Rev (5′-TCTAGATCATGCTTCGAATGTGAAATT-3′), GSTe9-Fwd (5′-CATATGATGGGAAAATTAGTACTGTACGG-3′), GSTe9-Rev (5′-TCTAGATTACACAATCTTTGTGATCTTCG-3′), agnobo-Fwd (5′-GGTACCATGATTCTGTACTACGACGAGGTCAGC-3′), and agnobo-Rev (5′-AAGCTTCTACAGCTTAATCTTTCCCGCTAAATG-3′). The *nobo* CDS was subcloned between the *Nde*I and *Xho*I restriction enzyme sites in pCold-III to generate the pCold-III_DmNobo[WT] vector. The *gste6* and *gste9* CDSs were subcloned between the *Nde*I and *Xba*I sites in pCold-III. It should be noted that pCold-III added a translation enhancing element (MNHKV) at the N-terminus of each of DmNobo, DmGSTE6 and DmGSTE9 proteins.

Expression vectors for DmNobo[Asp113Ala] and AgNobo[Asp111Ala] were constructed by inverse-PCR-based site-directed mutagenesis. The entire pCold-III_DmNobo[WT] and pCold-III_AgNobo[WT] plasmids were amplified by inverse PCR using a KOD-Plus-Mutagenesis Kit (Toyobo Co., Ltd, Osaka, Japan) using pairs of the oligonucleotides, 5′-CCAGTGATTTTATGTCGGCGATTGTCCGCC-3′ and 5′-CACGTCGGAACAAAAAGGAGCATTCGAAGA-3′ for DmNobo[Asp113Ala], and 5′-CGCTGCGGAAGTTATGCGTAAAATC-3′ and 5′-CGCTGAAACAAACAGCCGTTGTTG-3′ for AgNobo[Asp111Ala], as amplification primers. The *E. coli* strain DH5α was transformed with the *Dpn* I-digested PCR product. The plasmids were purified using a FastGene Plasmid Mini Kit (NIPPON Genetics Co., Ltd., Tokyo, Japan). Those DNA sequences

were confirmed by Sanger sequencing with one of the following sequencing primers: 5′-ACGCCATATCGCCGAAAGG-3′ or 5′-GGCAGGGATCTTAGATTCTG-3′.

DmNobo, AgNobo, *D. melanogaster* GSTE6 (DmGSTE6) and *D. melanogaster* GSTE9 (DmGSTE9) were expressed in the *E. coli* strain BL21(DE3) (Merck, Darmstadt, Germany) and purified via GSH-affinity column chromatography, followed by size-exclusion column chromatography. *E. coli* BL21(DE3) cells were transformed with pCold-III_DmNobo, and then the transformed cells were cultured in LB medium supplemented with 50 μg/mL ampicillin at 37°C. When the OD_{600} of the culture reached approximately 0.6, protein expression was induced with 0.3 mM isopropyl β-D-1-thiogalactopyranoside. The *E. coli* cells were cultured at 18°C overnight and then harvested. The harvested cells were suspended in lysis buffer (300 mM NaCl, 25 mM Tris-HCl, 1 mM CHAPS, 1 mM DTT, pH 8.0) and lysed for 2 min by sonication using a VP-305 Ultra 5 Homogenizer (TAITEC), using an output of 7 and a duty of 40%. The lysate was fractionated by centrifugation at 15,000 × *g* for 30 min at 4°C, and the supernatant was applied to a GSH-affinity column containing a 10-ml bed volume of glutathione Sepharose 4B (GE Healthcare, Little Chalfont, United Kingdom). After the column was washed with lysis buffer, the proteins were eluted with 50 ml of elution buffer (140 mM NaCl, 25 mM Tris-HCl [pH 8.0], 1 mM CHAPS, 1 mM DTT, 10 mM GSH). The eluent for DmNobo[Asp113Ala] was concentrated to 2 mL and fractionated with a Superdex200 increase 10/300 size-exclusion column (GE Healthcare) connected to an ÄKTA FPLC system (GE Healthcare) or those for DmNobo[WT], DmGSTE6, DmGSTE9 AgNobo[WT], and AgNobo[Asp111Ala] were concentrated to 5 ml and fractionated with HiLoad Superdex 200 16/600 column (GE Healthcare) . The columns were equilibrated with a buffer (150 mM NaCl, 25 mM Tris-HCl [pH 8.0], 1 mM DTT). DmNobo[Asp113Ala] protein was eluded with the same buffer at a flow rate of 0.2 mL/min and others were eluted at a flow rate of 1.0 mL/min. Purity and quality of final products were validated by SDS-PAGE and Coomassie Brilliant Blue staining. The peak fractions were concentrated to 15 mg/ml and stored at -80°C. The protein concentrations of DmNobo, DmGSTE6, DmGSTE9, and AgNobo was measured with a NanoDrop ND-1000 spectrophotometer (Thermo Fisher Scientific,

Massachusetts, United States of America) using extinction coefficients (ε_{280}) of 0.671 M^{-1}•cm^{-1}, 1.274 M^{-1}•cm^{-1}, 1.128 M^{-1}•cm^{-1}, and 1.100 M^{-1}•cm^{-1} respectively.

Crystallization

The Protein Crystallization System (Hiraki et al. 2006) was used for the initial crystallization screening of DmNobo (16). In total, 384 conditions were examined using the Crystal Screen 1 & 2, Index, PEG/Ion, or PEG/Ion 2 kits from Hampton Research (CA, USA), or the Wizard I & II kit from Molecular Dimensions (Suffolk, United Kingdom). DmNobo was crystallized at 20°C in the presence of 25% (w/v) PEG 3350 in 100 mM Bis-Tris (pH 5.5; index #42), or 45% (v/v) PPG 400 in 100 mM Bis-Tris (pH 6.5; index #58). The crystallization conditions were optimized by changing the pH and the concentration of the precipitation agent, resulting in two types of crystals, DmNobo I and II. DmNobo I crystals were obtained from a buffered solution containing 27.5% (w/v) PEG 3350 in 100 mM MES-NaOH (pH 5.4), and DmNobo II crystals were obtained from a buffered solution containing 42.5% (v/v) PPG400 in 100 mM Bis-Tris (pH 6.4). Crystals of substrate complexes were prepared by soaking the DmNobo II crystals in an artificial mother liquor (42.5% [w/v] PPG 400 in 100 mM Bis-Tris [pH 6.4]) containing 10 mM EST, with or without 1 mM GSH, for 6 h.

Crystal structure determinations

Crystals were picked up with proper size of MicroLoops (MiTeGen, New York, USA), flash frozen in liquid nitrogen, and packed in Uni-pucks (Molecular Dimensions). Diffraction data were collected at beamline BL-1A in the Photon Factory (Tsukuba, Japan) and at beamline X06SA in the Swiss Light Source. The diffraction datasets collected at the Photon Factory were automatically processed and scaled using XDS (Kabsch 2010), POINTLESS (Evans 2006), and AIMLESS (Evans and Murshudov 2013) on PReMo (Yamada et al. 2013), and those collected at the Swiss Light Source were processed and scaled using XDS and AIMLESS. Crystallographic statistics are summarized in Table 1-1.

Phases for DmNobo_Apo_1 (PDB ID: 6KEL) data collected from DmNobo I crystals were determined by the molecular replacement (MR) method with MOLREP (Vagin and Teplyakov 1997) using the crystal structure

of DmGSTE7 (PDB ID = 4PNG) as a search model. Other crystal structures were determined by the MR method using the crystal structure of DmNobo_Apo_1 as a search model. Molecular models were initially refined with REFMAC5 (Murshudov, Vagin, and Dodson 1997). The models were manually built using COOT (Emsley et al. 2010) and further refined with PHENIX.REFINE (Afonine et al. 2012) repeatedly. The C-terminal four residues could not be modeled due to poor electron density. In this study, the crystal structure of DmNobo_Apo_2 (PDB ID: 6KEM) determined with a DmNobo II crystal was used as the DmNobo_Apo structure when making comparisons with other crystal structures. m*F*o-D*F*c omit-maps for ligands were calculated using PHENIX.REFINE with a simulated annealing protocol. Interactions between DmNobo and GSH or EST was analyzed using PISA (Krissinel and Henrick 2007). The volume of the cavity in DmNobo was calculated using the Channel Finder program in 3V (Voss and Gerstein 2010), with 4-Å radius for the outer probe and a 1-Å radius for the inner probe. The volumes of GSH or EST were calculated using the Volume Assessor program in 3V, with a 2-Å radius for each probe. The RMSD from a least-squares fitting among the DmNobo structures was calculated with GESAMT (Krissinel 2012). Atom pairs within a 4.0-Å distance were defined as making direct contacts. All molecular graphics were prepared using the PyMOL Molecular Graphics System, version 1.7.6 (Schrödinger, NY, USA).

In vitro GST assay

In vitro GST assays with 3,4-DNADCF were performed as described previously (Fujikawa et al. 2015). The stock solutions of DmNobo[WT] and DmNobo[Asp113Ala] were 200 ng/mL each in solution A (2 mM GSH, 100 mM sodium phosphate buffer [pH 6.5], 0.01% Tween 20). Decreasing concentrations of DmNobo[WT] and DmNobo[Asp113Ala], ranging from 200 ng/mL to 0.19 ng/mL, were prepared by 2-fold serial dilution with solution A. The DmNobo dilution series was mixed with an equal volume of solution B (100 mM sodium phosphate buffer [pH 6.5] with 2 μM 3,4-DNADCF in 0.2% DMSO as a co-solvent) in each well of a 96-well plate to initiate the catalytic reaction of DmNobo. The GSH-conjugated product was excited at 485 nm, and the fluorescence intensity at 535 nm ($F_{measured}$) was measured every 30 s for 20 min with an infinite 200 PRO instrument (Tecan, Zurich, Switzerland). The

fluorescence intensity (F_t) in the reaction mixture without DmNobo (F_{bg}) was subtracted as the background signal ($F_t = F_{measured} - F_{bg}$). The maximum fluorescence intensity (F_{max}) was the fluorescence intensity that was reached as a plateau. The amount of product in each well (P_t) at the measured time (t) was calculated as P_t (μmol) = F_t/F_{max} × 200 μL × 1 μmol/L. The rate of product formation (P_{rate}, μmol/min) was obtained by linear-least-squares fitting between P_t and t. The specific activity of DmNobo (μmol/min/mg-protein) was defined as P_{rate}/[protein concentration]. The assay was performed in triplicate.

GST activity-inhibition assay

EST was dissolved in DMSO to a concentration of 2.5 mM. The 2.5 mM EST solution was diluted to 50 μM EST in solution C (2 mM GSH, 100 mM sodium phosphate buffer, 0.01% Tween 20, 2% DMSO, and 50 ng/mL DmNobo[WT], 50 ng/mL DmNobo[Asp113Ala], 100 ng/mL AgNobo[WT], 100 ng/ml AgNobo[Asp111Ala], 35 ng/mL DmGSTE6, or 300 ng/mL DmGSTE9 [pH 6.5]). A dilution series of EST, ranging from 50 μM to 0.19 μM, was prepared by 2-fold serial dilution with solution C. One hundred microliters of each EST solution in the dilution series was mixed with an equivalent amount of solution B (100 mM sodium phosphate buffer [pH 6.5] and 2 μM 3,4-DNADCF in 0.2% DMSO) in each well of a 96-well plate. $F_{measured}$ values were measured after 3 min, as described in the "*In vitro* GST assay" section. The fluorescence intensity detected in the absence of EST and DmNobo (F_{bg}) was subtracted as the background in all experiments ($F = F_{measured} - F_{bg}$). F at 0 s (F_0) was subtracted from F at the measured time (s) ($F_t = F - F_0$).

The relative activity was calculated as $F_{30\_[I]}/F_{30\_[0]}$, where [I] and [0] indicate the EST concentrations. The relative activity was plotted against each EST concentration. A fitting curve was calculated based on a plot generated from the following equation when IC_{50} and Hill constant (n) were approximated as 1.00 and 1.00, respectively, using KaleidaGraph version 4.5.1 (Synergy Software, Reading, USA):

$$\text{Relative activity (\%)} = 1/(1 + \{[EST]/IC_{50})^n\}) \times 100$$

The IC_{50} value was estimated based on the fitting curve. The assay was performed in triplicate.

Phylogenetic analysis

Nineteen amino acid sequences of DmNobo or *Bombyx mori* Nobo orthologues were found using BLASTP (Altschul et al. 2008) to search the NCBI non-redundant protein database. In addition, a Nobo orthologue in *H. armigera* was found in the Uniprot Knowledgebase. The accession numbers were XP_021192638.1 for *Helicoverpa armigera* GSTE14-like isoform X2, A0A2W1BRE1 for *H. armigera* uncharacterized protein, XP_022126447.1 for *Pieris rapae* GSTE14-like, XP_022837694.1 for *Spodoptera litura* GSTE14-like isoform X2, PCG75296.1 for *Heliothis virescens* hypothetical protein B5V51_11931, XP_013196516.1 for *Amyelois transitella* GST1, XP_001658748.2 for *Aedes aegypti* GSTE14, XP_319963.1 for *Anopheles gambiae* GSTE8, KXJ68754.1 for *Aedes albopictus* hypothetical protein RP20_CCG001852, ETN60212.1 for *Anopheles darlingi* GSTE, KFB39334.1 for *Anopheles sinensis* AGAP009190-PA-like protein, XP_001868776.1 for *Culex quinquefasciatus*, KOB78695.1 for *Operophtera brumata* GST, AIL29314.1 for *Cnaphalocrocis medinalis* GSTE5 partial region, XP_014368559.1 for *Papilio machaon* GSTE14-like, XP_013137131.1 for *Papilio polytes* GST1-1-like, NP_001299034.1 for *Papilio xuthus* GST1-1, NP_001292431.1 for an uncharacterized protein *Plutella xylostella*, ABY66602.1 for *B. mori* GSTE14, and OWR47941.1 for *Danaus plexippus*. Two *nobo* orthologues were found for *H. armigera* in the database.

For phylogenetic analysis of insect GSTD/E/T proteins, previously described amino acid sequences were obtained from the Uniprot Knowledgebase, NCBI protein database, and MonarchBase (Agarwala et al. 2018; Bateman et al. 2017; Enya et al. 2014; Zhan and Reppert 2013). Amino acid sequences (503) were aligned with COBALT (Papadopoulos and Agarwala 2007), and the resulting sequence alignment was used for cluster analysis with CLANS (Frickey and Lupas 2004). A major cluster included 372 amino acid sequences, including those of GSTD/E/T proteins and other GST proteins. A phylogenetic tree was drawn with COBALT, using the 372 GSTs and a neighbor-joining algorithm. I identified 371 sequences with a Grishin-sequence difference of 0.9, including 151 GSTDs, 178 GSTEs, and 42 GSTTs. I also identified 21 Nobo proteins among the GSTEs.

To calculate the amino acid frequencies, the obtained alignment was manually edited based on the known crystal structures, using Jalview

(Waterhouse et al. 2009). The amino acid frequencies were calculated and illustrated with WebLOGO version 3.7.4 (Crooks et al. 2004).

SPR assay

Surface plasmon resonance was measured at 25°C using Biacore T200 instrument with a CM5 sensor chip (GE Healthcare). DmNobo[WT] or the DmNobo[Asp113Ala] protein was used as a ligand, and EST was used as an analyte in PBS containing 1% DMSO, in the presence or absence of 1 mM GSH as a running buffer.

The Biacore T200 system with a CM5 sensor chip was filled with the running buffer. The ligands were immobilized on the activated CM5 sensor chip in an acetate buffer (pH 5.0) using a purchased amine-coupling kit (GE Healthcare) to reach 6,500 resonance units. The same process was performed in the absence of proteins in one lane on the chip as a background lane.

An EST dilution series was prepared by serial dilution. An EST stock solution (100 mM EST in DMSO) was diluted with running buffer to a concentration of 20 μM. The 20 μM EST solution was serially diluted by two thirds with running buffer seventeen times, and the running buffer in the absence of EST was used as the 0-μM EST sample. The analyte was flowed onto the sensor chip for 60 s and allowed to dissociate for 180 s.

EST concentrations of 20.000, 13.333, 8.889, 5.926, 3.951, 2.634, 1.756, 1.171, 0.780, 0.520, 0.347, 0.231, 0.154, 0.103, 0.069, 0.046, 0.030, 0.020, and 0.014 μM were used to calculate its *K*d. The background was subtracted from the sensorgrams of the proteins-immobilized lanes (sensorgrams shown in Fig. 3B). The *K*d values of EST for DmNobo[WT] and DmNobo[Asp113Ala] were evaluated with Biacore T200 Evaluation Software, using data from triplicate assays.

FMO calculations

Ab initio FMO calculations (Fedorov and Kitaura 2009; Fedorov, Nagata, and Kitaura 2012; Tanaka et al. 2014) were performed on the crystal structures of the DmNobo_Apo, DmNobo_EST-GSH, DmNobo_GSH, and DmNobo_EST complexes. While DmNobo is a homodimer, only the monomeric structure was utilized for the FMO calculations. Inter-subunit interactions were therefore neglected in this study. The crystal structures were modified before performing

the FMO calculations. First, all crystal water molecules, except for one that interacts with the carbonyl oxygens of Glu in GSH and Pro58, and the Oγ atom of Ser56 of DmNobo (Fig. 2A, water in yellow), were deleted from the crystal structures. Second, assignment of the protonation state and the addition of hydrogen atoms were performed using the Protonate 3D function of the Molecular Operating Environment program package (Chemical Computing Group, Montreal, Canada). Note that the carboxyl group of Asp113 was assigned to be ionized. Then, energy minimization of hydrogen atoms was performed with the Amber10:EHT force field. The protonated states of His55 and His71 were assumed to be positively charged to form hydrogen bonds with GSH. Then, FMO calculations for the monomeric DmNobo structures were performed using ABINIT-MP software (Gonze et al. 2009; Nakano et al. 2006). The second-order Møller-Plesset perturbation (MP2) (Mochizuki et al. 2004; Mochizuki et al. 2004) method was used with the 6-31G* basis function as a theoretical calculation level; namely, the FMO-MP2/6-31G* level of theory was used. For the FMO calculations, DmNobo proteins and GSH were fragmented into amino acid units at bonds between the C and Cα atoms of the main-chain. Each EST and water molecule was treated as a single fragment. The fragmentation treatment makes it possible to easily calculate the electronic structure of the whole complex and the IFIEs. The obtained IFIEs were further decomposed into four energy components, i.e., the ES, EX, CT+mix, and DI components, using PIEDA (Fedorov and Kitaura 2007; Tsukamoto et al. 2015).

MD simulations

The structures of DmNobo[WT]_EST-GSH, DmNobo[Asp113Ala]_EST-GSH, and DmNobo_cholesterol-GSH, were processed to assign bond orders and hydrogenation. The ionization states of EST, cholesterol, and GSH at pH 7.0 ± 2.0 were predicted using Epik (Shelley et al. 2007), and H-bond optimization was conducted using PROPKA (Li, Robertson, and Jensen 2005). Energy minimization was performed in Maestro using the OPLS3 force field (Harder et al. 2016).

Preparation for MD simulations was conducted using the Molecular Dynamics System Setup Module of Maestro (Schrödinger, NY, USA). DmNobo[WT]_EST-GSH and DmNobo[Asp113Ala]_EST-GSH were subjected to energy minimization and placed in an orthorhombic box with a buffer

distance of 10 Å to create a hydration model, and the TIP3P water model (Madura et al. 2003) was used for the hydration model. NaCl (0.15 M) served as the counterion to neutralize the system.

The MD simulations were performed using Desmond software, version 2.3 (Schrödinger, NY, USA). The cut-off radii for van der Waals, and the time step, initial temperature, and pressure of the system were set to 9 Å, 2.0 fs, 300 K, and 1.01325 bar, respectively. The sampling interval during the simulation was set to 10 ps. Finally, we performed MD simulations using the NPT ensemble for 100 ns.

Transgenic *D. melanogaster* insects and genetics

D. melanogaster flies were reared on standard agar-cornmeal medium at 25°C under a 12 h/12 h light/dark cycle. The strain harboring the Asp113Ala point mutation (*nobo*$^{3\times FLAG\text{-}HA\text{-}D113A}$), as well as the control wild-type strain (*nobo*$^{3\times FLAG\text{-}HA\text{-}WT}$) were generated using a CRISPR-Cas9-mediated knock-in strategy (Bier et al. 2018). Briefly, in each case, the genome of the starter *yw* strain was cut at 2 sites around the *nobo* locus, and then homologous recombination occurred with appropriate plasmids carrying 5′- and 3′-homology arms and an N-terminal 3× FLAG-HA epitope tag. The pDCC6 plasmid was used for simultaneous expression of both the Cas9 gene and guide RNA (gRNA) (Gokcezade et al. 2014). The following primer pairs were annealed and then ligated to *Bbs* I-digested pDCC6, which led to the production of 3 different gRNA plasmids: 5′-CTTCGTTGGGCTGAGACATTAAGTT-3′ and 5′-AAACAACTTAATGTCTCAGCCCAAC-3′ for Cutter#1; 5′-CTTCGTTACGACGAGCGCAGTCCGC-3′ and 5′-AAACGCGGACTGCGCTCGTCGTAAC-3′ for Cutter#2; and 5′-CTTCGCCGACGTGACAGTGATTTTA-3′ and 5′-AAACTAAAATCACTGTCACGTCGGC-3′ for Cutter#3. The pUC19-based plasmids carrying the homology arms and epitope tags, designated pDonor[KI]-{CG4688_LA}:{3×FLAG/HA/nobo}:{CG4688_RA} and pDonor[KI]-{CG4688_LA}:{3×FLAG/HA/nobo*D113A}:{CG4688_RA}, respectively, were artificially synthesized by VectorBuilder, Inc (Chicago, IL, USA). To generate the *nobo*$^{3\times FLAG\text{-}HA\text{-}WT}$ strain, the Cutter#1, Cutter#2, and pDonor[KI]-

{CG4688_LA}:{3×FLAG/HA/nobo}:{CG4688_RA} plasmids were injected into *yw* embryos. To generate the *nobo*$^{3\times FLAG\text{-}HA\text{-}D113A}$ strain, the Cutter#1, Cutter#3, and pDonor[KI]-{CG4688_LA}:{3×FLAG/HA/nobo*D113A}:{CG4688_RA} plasmids were injected to *yw* embryos. The proper knock-in strains were identified and characterized, essentially as described previously (Kina et al. 2019). DNA sequences surrounding the knock-in regions were confirmed by Sanger sequencing.

I found that *nobo*$^{3\times FLAG\text{-}HA\text{-}WT}$-homozygous flies were fully viable, whereas *nobo*$^{3\times FLAG\text{-}HA\text{-}D113A}$-homozygous flies displayed embryonic lethality. We utilized *nobo*$^{3\times FLAG\text{-}HA\text{-}D113A}$-heterozygous and -homozygous embryos for cuticle preparation and immunostaining. To formally rule out the possibility that the embryonic lethality was due to anonymous deleterious mutations other than *nobo*$^{3\times FLAG\text{-}HA\text{-}D113A}$, I counted the number of trans-heterozygous flies with a *nobo* knock-out (*nobo*^{KO}) from a previous report (Enya et al. 2014), as follows. Heterozygous *nobo*$^{3\times FLAG\text{-}HA\text{-}WT}$, *nobo*$^{3\times FLAG\text{-}HA\text{-}D113A}$, and *nobo*-knock-out (*nobo*^{KO}) alleles were balanced with *CyO* carrying *Actin5C:gfp* cassette (*CyO-GFP)*. Either *nobo*$^{3\times FLAG\text{-}HA\text{-}WT}$*/CyO-GFP* flies or *nobo*$^{3\times FLAG\text{-}A\text{-}D113A}$*/CyO-GFP* flies were crossed with *nobo*^{KO}*/CyO-GFP* flies. The trans-heterozygous flies (*nobo*$^{3\times FLAG\text{-}HA\text{-}WT}$*/nobo*^{KO} or *nobo*$^{3\times FLAG\text{-}HA\text{-}D113A}$*/nobo*^{KO}) should exhibit no GFP signals. I found that GFP-negative *nobo*$^{3\times FLAG\text{-}HA\text{-}WT}$*/nobo*^{KO} embryos hatched normally and developed into adults without any abnormalities, whereas *nobo*$^{3\times FLAG\text{-}HA\text{-}D113A}$*/nobo*^{KO} embryos did not.

Cuticle preparation and immunostaining

Embryonic cuticle preparation was performed as previously described (Wieschaus and Nüsslein-Volhard 1986). Immunostaining for whole-mount embryos was conducted as previously described (Enya et al. 2014). A mouse anti-FasIII monoclonal antibody 7G10 (Developmental Studies Hybridoma Bank, University of Iowa, USA; 1:20 dilution) and an anti-mouse IgG antibody conjugated with Alexa488 (Life Technologies; 1:200 dilution) were used for immunostaining the embryos. For immunostaining of the brain-ring gland complex in third-instar larvae, we first crossed *nobo*$^{3\times FLAG\text{-}HA\text{-}WT}$ homozygous females or *nobo*$^{3\times FLAG\text{-}HA\text{-}D113A}$*/CyO-GFP* females with Oregon-R wild type males. Third-instar larvae of the heterozygous offspring (*nobo*$^{3\times FLAG\text{-}HA\text{-}WT}$/+ or *nobo*$^{3\times FLAG\text{-}HA\text{-}D113A}$/+) were dissected and then immunostained as

previously described (Imura et al. 2017). The antibodies used for the brain-ring gland complex included a rat anti-HA high-affinity monoclonal antibody (3F10, 1:20 dilution; Roche), a guinea pig anti-Shroud antibody (Shimada-Niwa and Niwa 2014) (1:200 dilution), an anti-rat IgG antibody conjugated with Alexa488 (1:200 dilution; Life Technologies), and an anti-guinea pig IgG antibody conjugated with Alexa555 (1:200 dilution; Life Technologies). Fluorescence images were obtained using an LSM700 microscope (Carl Zeiss).

Acknowledgments

I express my deep gratitude to Dr. Ryusuke Niwa for mentioning my research. I am honed to have worked with him and all members of the Physiological Dynamics Lab at TARA Center, University of Tsukuba.

I thank Dr. Fumiaki Yumoto, Dr. Kotaro Koiwai, Dr. Outa Uryu, and Ms. Kana Morohashi for their technical support.

I also thank the following people for collaborating with me in this work: Dr. Toshiya Senda, Dr. Fumiaki Yumoto, and Dr. Kotaro Koiwai for X-ray crystallography; Dr. Takatsugu Hirokawa and Dr. Ryunosuke Yoshino for MD simulation; Dr. Takayoshi Okabe, Dr. Hirotatsu Kojima, and Dr. Riyo Imamura for HTS; Dr. Hideshi Inoue and Dr. Yuta Fujikawa for providing 3,4-DNADCF; Dr. Yuko Shimada-Niwa for *Drosophila* immunostaining; Dr. Teruki Honma and Dr. Chiduru Watanabe for the first screening of inhibitors; Tamie Katsuta, Hiroyuki Matsumaru, and Dr. Ryuichi Kato for setting up the screening of crystallography conditions; Dr. Yusuke Yamada for managing the automated data collection at the Photon Factory; and Dr. Ayaka Harada, Dr. Akira Shinoda, and Dr. Miki Senda for data collection at the Swiss Light Source.

I thank Dr. Yuta Fujikawa, Dr. Hirotaka Kanuka, Dr. Chisako Sakuma, Dr. Akira Nakamura, and the Developmental Studies Hybridoma Bank for providing stocks and reagents.

I thank Dr. Yoshiaki Nakagawa, Dr. Hajime Ono, and Dr. Tetsuo Nagano for providing valuable feedback.

I thank Dr. Tomoki Chiba, Dr. Kentaro Nakano, and Dr. Tetsuo Hashimoto for taking part to my dissertation advisory committee.

I would like to thank Editage (www.editage.com) for English language editing.

This work was supported by a KEK Postgraduate Research Student fellowship, the KAKENHI (grant numbers 15K14719 and 18K19163 to R.N.), the Platform Project for Supporting in Drug Discovery and Life Science Research (Platform for Drug Discovery, Informatics, and Structural Life Science), and the Basis for Supporting Innovative Drug Discovery and Life Science Research from the Japan Agency for Medical Research and Development (AMED) under grant number 18am0101113j0002. This work was performed with the approval of the Photon Factory Program Advisory Committee (proposal number 2018G025).

References

Adolfi, Adriana, Beth Poulton, Amalia Anthousi, Stephanie Macilwee, Hilary Ranson, and Gareth J. Lycett. 2019. "Functional Genetic Validation of Key Genes Conferring Insecticide Resistance in the Major African Malaria Vector, Anopheles Gambiae." *Proceedings of the National Academy of Sciences of the United States of America* 116(51):25764–72.

Afonine, Pavel V, Ralf W. Grosse-Kunstleve, Nathaniel Echols, Jeffrey J. Headd, Nigel W. Moriarty, Marat Mustyakimov, Thomas C. Terwilliger, Alexandre Urzhumtsev, Peter H. Zwart, and Paul D. Adams. 2012. "Towards Automated Crystallographic Structure Refinement with Phenix.Refine." *Acta Crystallographica Section D: Biological Crystallography* 68(4):352–67.

Agarwala, Richa, Tanya Barrett, Jeff Beck, Dennis A. Benson, Colleen Bollin, Evan Bolton, Devon Bourexis, J. Rodney Brister, Stephen H. Bryant, Kathi Canese, Mark Cavanaugh, Chad Charowhas, Karen Clark, Ilya Dondoshansky, Michael Feolo, Lawrence Fitzpatrick, Kathryn Funk, Lewis Y. Geer, Viatcheslav Gorelenkov, Alan Graeff, Wratko Hlavina, Brad Holmes, Mark Johnson, Brandi Kattman, Viatcheslav Khotomlianski, Avi Kimchi, Michael Kimelman, Masato Kimura, Paul Kitts, William Klimke, Alex Kotliarov, Sergey Krasnov, Anatoliy Kuznetsov, Melissa J. Landrum, David Landsman, Stacy Lathrop, Jennifer M. Lee, Carl Leubsdorf, Zhiyong Lu, Thomas L. Madden, Aron Marchler-Bauer, Adriana Malheiro, Peter Meric, Ilene Karsch-Mizrachi, Anatoly Mnev, Terence Murphy, Rebecca Orris, James Ostell, Christopher O'Sullivan, Vasuki Palanigobu, Anna R. Panchenko, Lon Phan, Borys Pierov, Kim D. Pruitt, Kurt Rodarmer, Eric W. Sayers, Valerie Schneider, Conrad L. Schoch, Gregory D. Schuler, Stephen T. Sherry, Karanjit Siyan, Alexandra Soboleva, Vladimir Soussov, Grigory Starchenko, Tatiana A. Tatusova, Francoise Thibaud-Nissen, Kamen Todorov, Bart W. Trawick, Denis Vakatov, Minghong Ward, Eugene Yaschenko, Aleksandr Zasypkin, and Kerry Zbicz. 2018. "Database Resources of the National Center for Biotechnology Information." *Nucleic Acids Research* 46(D1):D8–13.

Al-Massarani, Shaza, Amina El-Shaibany, Nurhayat Tabanca, Abbas Ali, Alden S. Estep, James J. Becnel, Fatih Goger, Betul Demirci, Ali El-Gamal, and K. Husnu Can Baser. 2019. "Assessment of Selected Saudi and Yemeni Plants for Mosquitocidal Activities against the Yellow Fever Mosquito Aedes Aegypti." *Saudi Pharmaceutical Journal* 27(7):930–38.

Altschul, S. F., T. L. Madden, A. A. Schaffer, J. Zhang, Z. Zhang, W. Miller, and D. J. Lipman. 2008. *The Universal Protein Resource (UniProt)¥rGapped BLAST and PSI-BLAST: A New Generation of Protein Database Search Programs*.

Avvakumov, George V., Irina Grishkovskaya, Yves A. Muller, and Geoffrey L. Hammond. 2002. "Crystal Structure of Human Sex Hormone-Binding Globulin in Complex with 2-Methoxyestradiol Reveals the Molecular Basis for High Affinity Interactions with C-2 Derivatives of Estradiol." *Journal of Biological Chemistry* 277(47):45219–25.

Ayres, Constância, Pie Müller, Naomi Dyer, Craig Wilding, Daniel Rigden, and Martin Donnelly. 2011. "Comparative Genomics of the Anopheline Glutathione S-Transferase Epsilon Cluster." *PLoS ONE* 6(12).

Bateman, Alex, Maria Jesus Martin, Claire O'Donovan, Michele Magrane, Emanuele Alpi, Ricardo Antunes, Benoit Bely, Mark Bingley, Carlos Bonilla, Ramona Britto, Borisas Bursteinas, Hema Bye-AJee, Andrew Cowley, Alan Da Silva, Maurizio De Giorgi, Tunca Dogan, Francesco Fazzini, Leyla Garcia Castro, Luis Figueira, Penelope Garmiri, George Georghiou, Daniel Gonzalez, Emma Hatton-Ellis, Weizhong Li, Wudong Liu, Rodrigo Lopez, Jie Luo, Yvonne Lussi, Alistair MacDougall, Andrew Nightingale, Barbara Palka, Klemens Pichler, Diego Poggioli, Sangya Pundir, Luis Pureza, Guoying Qi, Steven Rosanoff, Rabie Saidi, Tony Sawford, Aleksandra Shypitsyna, Elena Speretta, Edward Turner, Nidhi Tyagi, Vladimir Volynkin, Tony Wardell, Kate Warner, Xavier Watkins, Rossana Zaru, Hermann Zellner, Ioannis Xenarios, Lydie Bougueleret, Alan Bridge, Sylvain Poux, Nicole Redaschi, Lucila Aimo, Ghislaine ArgoudPuy, Andrea Auchincloss, Kristian Axelsen, Parit Bansal, Delphine Baratin, Marie Claude Blatter, Brigitte Boeckmann, Jerven Bolleman,

Emmanuel Boutet, Lionel Breuza, Cristina Casal-Casas, Edouard De Castro, Elisabeth Coudert, Beatrice Cuche, Mikael Doche, Dolnide Dornevil, Severine Duvaud, Anne Estreicher, Livia Famiglietti, Marc Feuermann, Elisabeth Gasteiger, Sebastien Gehant, Vivienne Gerritsen, Arnaud Gos, Nadine Gruaz-Gumowski, Ursula Hinz, Chantal Hulo, Florence Jungo, Guillaume Keller, Vicente Lara, Philippe Lemercier, Damien Lieberherr, Thierry Lombardot, Xavier Martin, Patrick Masson, Anne Morgat, Teresa Neto, Nevila Nouspikel, Salvo Paesano, Ivo Pedruzzi, Sandrine Pilbout, Monica Pozzato, Manuela Pruess, Catherine Rivoire, Bernd Roechert, Michel Schneider, Christian Sigrist, Karin Sonesson, Sylvie Staehli, Andre Stutz, Shyamala Sundaram, Michael Tognolli, Laure Verbregue, Anne Lise Veuthey, Cathy H. Wu, Cecilia N. Arighi, Leslie Arminski, Chuming Chen, Yongxing Chen, John S. Garavelli, Hongzhan Huang, Kati Laiho, Peter McGarvey, Darren A. Natale, Karen Ross, C. R. Vinayaka, Qinghua Wang, Yuqi Wang, Lai Su Yeh, and Jian Zhang. 2017. "UniProt: The Universal Protein Knowledgebase." *Nucleic Acids Research* 45(D1):D158–69.

Bier, Ethan, Melissa M. Harrison, Kate M. O'connor-Giles, and Jill Wildonger. 2018. "Advances in Engineering the Fly Genome with the CRISPR-Cas System." *Genetics*.

Brzozowski, Andrzej M., Ashley C. W. Pike, Zbigniew Dauter, Roderick E. Hubbard, Tomas Bonn, Owe Engström, Lars Öhman, Geoffrey L. Greene, Jan Åke Gustafsson, and Mats Carlquist. 1997. "Molecular Basis of Agonism and Antagonism in the Oestrogen Receptor." *Nature* 389(6652):753–58.

Chanut-Delalande, Hélène, Yoshiko Hashimoto, Anne Pelissier-Monier, Rebecca Spokony, Azza Dib, Takefumi Kondo, Jérôme Bohère, Kaori Niimi, Yvan Latapie, Sachi Inagaki, Laurence Dubois, Philippe Valenti, Cédric Polesello, Satoru Kobayashi, Bernard Moussian, Kevin P. White, Serge Plaza, Yuji Kageyama, and François Payre. 2014. "Pri Peptides Are Mediators of Ecdysone for the Temporal Control of Development." *Nature Cell Biology* 16(11):1035–44.

Chavez, V. M., G. Marques, J. P. Delbecque, K. Kobayashi, M. Hollingsworth, J. Burr, J. E. Natzle, and M. B. O'Connor. 2000. "The Drosophila Disembodied Gene Controls Late Embryonic Morphogenesis and Codes for a Cytochrome P450 Enzyme That Regulates Embryonic Ecdysone Levels." *Development* 127(19):4115–26.

Che-Mendoza, Azael, R. Patricia Penilla, and D. Américo Rodriguez. 2009. "Insecticide Resistance and Glutathione S-Transferases in Mosquitoes: A Review." *African Journal of Biotechnology* 8(8):1386–97.

Coon, Kerri L., Luca Valzania, David A. McKinney, Kevin J. Vogel, Mark R. Brown, and Michael R. Strand. 2017. "Bacteria-Mediated Hypoxia Functions as a Signal for Mosquito Development." *Proceedings of the National Academy of Sciences* 114(27):E5362–69.

Crooks, Gavin E., Gary Hon, John Marc Chandonia, and Steven E. Brenner. 2004. "WebLogo: A Sequence Logo Generator." *Genome Research*.

Emsley, P., B. Lohkamp, W. G. Scott, and K. Cowtan. 2010. "Features and Development of Coot." *Acta Crystallographica Section D: Biological Crystallography* 66(4):486–501.

Enya, Sora, Tomotsune Ameku, Fumihiko Igarashi, Masatoshi Iga, Hiroshi Kataoka, Tetsuro Shinoda, and Ryusuke Niwa. 2014. "A Halloween Gene Noppera-Bo Encodes a Glutathione S-Transferase Essential for Ecdysteroid Biosynthesis via Regulating the Behaviour of Cholesterol in Drosophila." *Scientific Reports* 4(6586):1–10.

Enya, Sora, Takaaki Daimon, Fumihiko Igarashi, Hiroshi Kataoka, Miwa Uchibori, Hideki Sezutsu, Tetsuro Shinoda, and Ryusuke Niwa. 2015. "The Silkworm Glutathione S-Transferase Gene Noppera-Bo Is Required for Ecdysteroid Biosynthesis and Larval Development." *Insect Biochemistry and Molecular Biology* 61:1–7.

Enya, Sora, Chikana Yamamoto, Hajime Mizuno, Tsuyoshi Esaki, Hsin-Kuang Lin, Masatoshi Iga, Kana Morohashi, Yota Hirano, Hiroshi Kataoka, Tsutomu Masujima, Yuko Shimada-Niwa, and Ryusuke Niwa. 2017. "Dual Roles of Glutathione in Ecdysone Biosynthesis and Antioxidant Function

During the Larval Development in *Drosophila*." *Genetics* 207(December):genetics.300391.2017.

Evans, Philip. 2006. "Scaling and Assessment of Data Quality." *Acta Crystallographica Section D: Biological Crystallography* 62(1):72–82.

Evans, Philip R. and Garib N. Murshudov. 2013. "How Good Are My Data and What Is the Resolution?" *Acta Crystallographica Section D: Biological Crystallography* 69(7):1204–14.

Federici, Luca, Carlo Lo Sterzo, Silvia Pezzola, Adele Di Matteo, Flavio Scaloni, Giorgio Federici, and Anna Maria Caccuri. 2009. "Structural Basis for the Binding of the Anticancer Compound 6-(7-Nitro-2,1,3-Benzoxadiazol-4-Ylthio)Hexanol to Human Glutathione S-Transferases." *Cancer Research* 69(20):8025–34.

Fedorov, Dmitri G. and Kazuo Kitaura. 2007. "Pair Interaction Energy Decomposition Analysis." *Journal of Computational Chemistry*.

Fedorov, Dmitri G., Takeshi Nagata, and Kazuo Kitaura. 2012. "Exploring Chemistry with the Fragment Molecular Orbital Method." *Physical Chemistry Chemical Physics*.

Fedorov, Dmitri and Kazuo Kitaura. 2009. *The Fragment Molecular Orbital Method*. Taylor & Francis Group, 6000 Broken Sound Parkway NW, Suite 300, Boca Raton, FL 33487-2742: CRC Press.

Frickey, Tancred and Andrei Lupas. 2004. "CLANS: A Java Application for Visualizing Protein Families Based on Pairwise Similarity." *Bioinformatics* 20(18):3702–4.

Fujikawa, Yuuta, Fumika Morisaki, Asami Ogura, Kana Morohashi, Sora Enya, Ryusuke Niwa, Shinji Goto, Hirotatsu Kojima, Takayoshi Okabe, Tetsuo Nagano, and Hideshi Inoue. 2015. "A Practical Fluorogenic Substrate for High-Throughput Screening of Glutathione S-Transferase Inhibitors." *Chem. Commun.* 51(57):11459–62.

Fukuzawa, Kaori, Yuji Mochizuki, Shigenori Tanaka, Kazuo Kitaura, and Tatsuya Nakano. 2006. "Molecular Interactions between Estrogen Receptor and Its Ligand Studied by the Ab Initio Fragment Molecular Orbital Method." *Journal of Physical Chemistry B* 110(32):16102–10.

Gilbert, Lawrence I. 2004. "Halloween Genes Encode P450 Enzymes That Mediate Steroid Hormone Biosynthesis in Drosophila Melanogaster." *Molecular and Cellular Endocrinology* 215(1–2):1–10.

Gokcezade, J., G. Sienski, and P. Duchek. 2014. "Efficient CRISPR/Cas9 Plasmids for Rapid and Versatile Genome Editing in Drosophila." *G3* 4(11):2279–82.

Gonze, X., B. Amadon, P. M. Anglade, J. M. Beuken, F. Bottin, P. Boulanger, F. Bruneval, D. Caliste, R. Caracas, M. Côté, T. Deutsch, L. Genovese, Ph Ghosez, M. Giantomassi, S. Goedecker, D. R. Hamann, P. Hermet, F. Jollet, G. Jomard, S. Leroux, M. Mancini, S. Mazevet, M. J. T. Oliveira, G. Onida, Y. Pouillon, T. Rangel, G. M. Rignanese, D. Sangalli, R. Shaltaf, M. Torrent, M. J. Verstraete, G. Zerah, and J. W. Zwanziger. 2009. "ABINIT: First-Principles Approach to Material and Nanosystem Properties." *Computer Physics Communications*.

Gu, Yijun, Jianxia Guo, Ajay Pal, Su Shu Pan, Piotr Zimniak, Shivendra V. Singh, and Xinhua Ji. 2004. "Crystal Structure of Human Glutathione S-Transferase A3-3 and Mechanistic Implications for Its High Steroid Isomerase Activity." *Biochemistry* 43(50):15673–79.

Harder, Edward, Wolfgang Damm, Jon Maple, Chuanjie Wu, Mark Reboul, Jin Yu Xiang, Lingle Wang, Dmitry Lupyan, Markus K. Dahlgren, Jennifer L. Knight, Joseph W. Kaus, David S. Cerutti, Goran Krilov, William L. Jorgensen, Robert Abel, and Richard A. Friesner. 2016. "OPLS3: A Force Field Providing Broad Coverage of Drug-like Small Molecules and Proteins." *Journal of Chemical Theory and Computation* 12(1):281–96.

Harris, Heather A., Ashok R. Bapat, Daniel S. Gonder, and Donald E. Frail. 2002. "The Ligand Binding Profiles of Estrogen Receptors α and β Are Species Dependent." *Steroids* 67(5):379–84.

Helvecio, Elisama, Tatiany Patrícia Romão, Danilo de Carvalho-Leandro, Iêda Ferreira de Oliveira, Antonio Emanuel Holanda D. Cavalcanti, Lisa Reimer, Milena de Paiva Cavalcanti, Ana Patrícia Silva de Oliveira, Patrícia Maria Guedes Paiva, Thiago Henrique Napoleão, Gabriel Luz Wallau, Osvaldo P. de Melo Neto, Maria Alice Varjal Melo-Santos, and Constância

Flávia Junqueira Ayres. 2020. "Polymorphisms in GSTE2 Is Associated with Temephos Resistance in Aedes Aegypti." *Pesticide Biochemistry and Physiology* 165(September 2019):104464.

Hiraki, Masahiko, Ryuichi Kato, Minoru Nagai, Tadashi Satoh, Satoshi Hirano, Kentaro Ihara, Norio Kudo, Masamichi Nagae, Masanori Kobayashi, Michio Inoue, Tamami Uejima, Shunichiro Oda, Leonard M. G. Chavas, Masato Akutsu, Yusuke Yamada, Masato Kawasaki, Naohiro Matsugaki, Noriyuki Igarashi, Mamoru Suzuki, and Soichi Wakatsuki. 2006. "Development of an Automated Large-Scale Protein-Crystallization and Monitoring System for High-Throughput Protein-Structure Analyses." *Acta Crystallographica Section D: Biological Crystallography* 62(9):1058–65.

Imura, Eisuke, Yuto Yoshinari, Yuko Shimada-Niwa, and Ryusuke Niwa. 2017. "Protocols for Visualizing Steroidogenic Organs and Their Interactive Organs with Immunostaining in the Fruit Fly Drosophila Melanogaster." *Journal of Visualized Experiments* (122).

Kabsch, Wolfgang. 2010. "Xds." *Acta Crystallographica Section D: Biological Crystallography* 66(2):125–32.

Kabsch, Wolfgang, Brünger A. T., Diederichs K., Karplus P. A., Diederichs K., McSweeney S., Ravelli R. B. G., Evans P., French S., Wilson K., Kabsch W., Kabsch W., Kabsch W., Kabsch W., Kursula P., and Weiss M. S. 2010. "*XDS*." *Acta Crystallographica Section D Biological Crystallography* 66(2):125–32.

Kina, Hiroko, Takashi Yoshitani, Kazuko Hanyu-Nakamura, and Akira Nakamura. 2019. "Rapid and Efficient Generation of GFP-knocked-in Drosophilaby the CRISPR-Cas9-mediated Genome Editing." *Develop. Growth Differ.* 61:265–275.

Koiwai, Kotaro, Kazue Inaba, Kana Morohashi, Sora Enya, Reina Arai, Hirotatsu Kojima, Takayoshi Okabe, Yuuta Fujikawa, Hideshi Inoue, Ryunosuke Yoshino, Takatsugu Hirokawa, Koichiro Kato, Kaori Fukuzawa, Yuko Shimada-Niwa, Akira Nakamura, Fumiaki Yumoto, Toshiya Senda, and Ryusuke Niwa. 2020. "An Integrated Approach to Unravel a Crucial

Structural Property Required for the Function of the Insect Steroidogenic Halloween Protein Noppera-Bo." *Journal of Biological Chemistry* 295(20):7154–67.

Krissinel, Evgeny. 2012. "Enhanced Fold Recognition Using Efficient Short Fragment Clustering." *Journal of Molecular Biochemistry* 1(2):76–85.

Krissinel, Evgeny and Kim Henrick. 2007. "Inference of Macromolecular Assemblies from Crystalline State." 774–97.

Li, Hui, Andrew D. Robertson, and Jan H. Jensen. 2005. "Very Fast Empirical Prediction and Rationalization of Protein PK a Values." *Proteins: Structure, Function and Genetics* 61(4):704–21.

Low, Wai Yee, Susanne C. Feil, Hooi Ling Ng, Michael A. Gorman, Craig J. Morton, James Pyke, Malcolm J. McConville, Michael Bieri, Yee Foong Mok, Charles Robin, Paul R. Gooley, Michael W. Parker, and Philip Batterham. 2010. "Recognition and Detoxification of the Insecticide DDT by Drosophila Melanogaster Glutathione S-Transferase D1." *Journal of Molecular Biology* 399(3):358–66.

Lumjuan, Nongkran, Lynn McCarroll, La Aied Prapanthadara, Janet Hemingway, and Hilary Ranson. 2005. "Elevated Activity of an Epsilon Class Glutathione Transferase Confers DDT Resistance in the Dengue Vector, Aedes Aegypti White Star." *Insect Biochemistry and Molecular Biology* 35(8):861–71.

Madura, Jeffry D., William L. Jorgensen, Jayaraman Chandrasekhar, Michael L. Klein, and Roger W. Impey. 2003. "Comparison of Simple Potential Functions for Simulating Liquid Water." *The Journal of Chemical Physics* 79(2):926–35.

Manas, Eric S., Zhang B. Xu, Rayomand J. Unwalla, and William S. Somers. 2004. "Understanding the Selectivity of Genistein for Human Estrogen Receptor-β Using X-Ray Crystallography and Computational Methods." *Structure* 12(12):2197–2207.

Martelli, Felipe, Zuo Zhongyuan, Julia Wang, Ching On Wong, Nicholas E. Karagas, Ute Roessner, Thusitha Rupasinghe, Kartik Venkatachalam, Trent Perry, Hugo J. Bellen, and Philip Batterham. 2020. "Low Doses of

the Neonicotinoid Insecticide Imidacloprid Induce ROS Triggering Neurological and Metabolic Impairments in Drosophila." *Proceedings of the National Academy of Sciences of the United States of America* 117(41):25840–50.

Mashiyama, Susan T., M. Merced Malabanan, Eyal Akiva, Rahul Bhosle, Megan C. Branch, Brandan Hillerich, Kevin Jagessar, Jungwook Kim, Yury Patskovsky, Ronald D. Seidel, Mark Stead, Rafael Toro, Matthew W. Vetting, Steven C. Almo, Richard N. Armstrong, and Patricia C. Babbitt. 2014. "Large-Scale Determination of Sequence, Structure, and Function Relationships in Cytosolic Glutathione Transferases across the Biosphere." *PLoS Biology* 12(4).

Mbachu, Obinna C., Caitlin Howell, Charlotte Simmler, Gonzalo R. Malca Garcia, Kornelia J. Skowron, Huali Dong, Sarah G. Ellis, Ryan T. Hitzman, Atieh Hajirahimkhan, Shao Nong Chen, Dejan Nikolic, Terry W. Moore, Günter Vollmer, Guido F. Pauli, Judy L. Bolton, and Birgit M. Dietz. 2020. "SAR Study on Estrogen Receptor α/β Activity of (Iso)Flavonoids: Importance of Prenylation, c-Ring (Un)Saturation, and Hydroxyl Substituents." *Journal of Agricultural and Food Chemistry* 68(39):10651–63.

Mochizuki, Yuji, Shigeru Koikegami, Tatsuya Nakano, Shinji Amari, and Kazuo Kitaura. 2004. "Large Scale MP2 Calculations with Fragment Molecular Orbital Scheme." *Chemical Physics Letters*.

Mochizuki, Yuji, Tatsuya Nakano, Shigeru Koikegami, Souichirou Tanimori, Yukinobu Abe, Umpei Nagashima, and Kazuo Kitaura. 2004. "A Parallelized Integral-Direct Second-Order Møller-Plesset Perturbation Theory Method with a Fragment Molecular Orbital Scheme." *Theoretical Chemistry Accounts*.

Morou, Evangelia, Andrew J. Dowd, Shavanti Rajatileka, Andrew Steven, Janet Hemingway, Hilary Ranson, Mark Paine, and John Vontas. 2010. "A Simple Colorimetric Assay for Specific Detection of Glutathione-S Transferase Activity Associated with DDT Resistance in Mosquitoes." *PLoS Neglected Tropical Diseases* 4(8):1–6.

Moyes, Catherine L., John Vontas, Ademir J. Martins, Lee Ching Ng, Sin Ying Koou, Isabelle Dusfour, Kamaraju Raghavendra, João Pinto, Vincent Corbel, Jean Philippe David, and David Weetman. 2017. "Contemporary Status of Insecticide Resistance in the Major Aedes Vectors of Arboviruses Infecting Humans." *PLoS Neglected Tropical Diseases* 11(7):1–20.

Murata, Mariko, Kaoru Midorikawa, Masashi Koh, Kazuo Umezawa, and Shosuke Kawanishi. 2004. "Genistein and Daidzein Induce Cell Proliferation and Their Metabolites Cause Oxidative DNA Damage in Relation to Isoflavone-Induced Cancer of Estrogen-Sensitive Organs." *Biochemistry* 43(9):2569–77.

Murshudov, G. N., A. A. Vagin, and E. J. Dodson. 1997. "Refinement of Macromolecular Structures by the Maximum-Likelihood Method." *Acta Crystallographica Section D Biological Crystallography* 53(3):240–55.

Nakagawa, Yoshiaki and Vincent C. Henrich. 2009. "Arthropod Nuclear Receptors and Their Role in Molting." *FEBS Journal* 276(21):6128–57.

Nakano, Tatsuya, Yuji Mochizuki, Kaori Fukuzawa, Shinji Amari, and Shigenori Tanaka. 2006. "Developments and Applications of ABINIT-MP Software Based on the Fragment Molecular Orbital Method." in *Modern Methods for Theoretical Physical Chemistry of Biopolymers*.

Namiki, Toshiki, Ryusuke Niwa, Takashi Sakudoh, Ken Ichi Shirai, Hideaki Takeuchi, and Hiroshi Kataoka. 2005. "Cytochrome P450 CYP307A1/Spook: A Regulator for Ecdysone Synthesis in Insects." *Biochemical and Biophysical Research Communications* 337(1):367–74.

Niwa, R., T. Matsuda, T. Yoshiyama, T. Namiki, K. Mita, Y. Fujimoto, and H. Kataoka. 2004. "CYP306A1, a Cytochrome P450 Enzyme, Is Essential for Ecdysteroid Biosynthesis in the Prothoracic Glands of Bombyx and Drosophila." *J Biol Chem* 279(34):35942–49.

Niwa, R., T. Namiki, K. Ito, Y. Shimada-Niwa, M. Kiuchi, S. Kawaoka, T. Kayukawa, Y. Banno, Y. Fujimoto, S. Shigenobu, S. Kobayashi, T. Shimada, S. Katsuma, and T. Shinoda. 2010. "Non-Molting Glossy/Shroud Encodes a Short-Chain Dehydrogenase/Reductase That Functions in the

'Black Box' of the Ecdysteroid Biosynthesis Pathway." *Development* 137(12):1991–99.

Niwa, Ryusuke and Yuko S. Niwa. 2014. "Enzymes for Ecdysteroid Biosynthesis: Their Biological Functions in Insects and Beyond." *Bioscience, Biotechnology and Biochemistry* 78(8):1283–92.

Niwa, Yuko S. and Ryusuke Niwa. 2016. "Transcriptional Regulation of Insect Steroid Hormone Biosynthesis and Its Role in Controlling Timing of Molting and Metamorphosis." *Development Growth and Differentiation* 58(1):94–105.

O Duke, Stephen and Stephen B Powles. 2008. "Chitin Synthesis Inhibitor Effect on Aedes Aegypti Populations Susceptible and Resistant to Organophosphate Temephos." *Pest Management Science* 63(11):676–80.

Ono, Hajime, Kim F. Rewitz, Tetsuro Shinoda, Kyo Itoyama, Anna Petryk, Robert Rybczynski, Michael Jarcho, James T. Warren, Guillermo Marqués, Mary Jane Shimell, Lawrence I. Gilbert, and Michael B. O'Connor. 2006. "Spook and Spookier Code for Stage-Specific Components of the Ecdysone Biosynthetic Pathway in Diptera." *Developmental Biology* 298(2):555–70.

Ou, Qiuxiang, Adam Magico, and Kirst King-Jones. 2011. "Nuclear Receptor DHR4 Controls the Timing of Steroid Hormone Pulses during Drosophila Development." *PLoS Biology* 9(9):e1001160.

Papadopoulos, Jason S. and Richa Agarwala. 2007. "COBALT: Constraint-Based Alignment Tool for Multiple Protein Sequences." *Bioinformatics*.

Pedersen, Lars C., Evgeniy Petrotchenko, Sergei Shevtsov, and Masahiko Negishi. 2002. "Crystal Structure of the Human Estrogen Sulfotransferase-PAPS Complex." *Journal of Biological Chemistry* 277(20):17928–32.

Perperopoulou, Fereniki, Fotini Pouliou, and Nikolaos E. Labrou. 2018. "Recent Advances in Protein Engineering and Biotechnological Applications of Glutathione Transferases." *Critical Reviews in Biotechnology* 38(4):511–28.

Petryk, A., J. T. Warren, G. Marques, M. P. Jarcho, L. I. Gilbert, J. Kahler, J. P. Parvy, Y. Li, C. Dauphin-Villemant, and M. B. O'Connor. 2003. "Shade Is the Drosophila P450 Enzyme That Mediates the Hydroxylation of Ecdysone to the Steroid Insect Molting Hormone 20-Hydroxyecdysone." *Proceedings of the National Academy of Sciences* 100(24):13773–78.

Pike, Ashley C. W., Andrzej M. Brzozowski, Roderick E. Hubbard, Tomas Bonn, Ann Gerd Thorsell, Owe Engström, Jan Ljunggren, Jan Åke Gustafsson, and Mats Carlquist. 1999. "Structure of the Ligand-Binding Domain of Oestrogen Receptor Beta in the Presence of a Partial Agonist and a Full Antagonist." *EMBO Journal* 18(17):4608–18.

Pinto, Patricia I. S., Maria D. Estêvão, and Deborah M. Power. 2014. "Effects of Estrogens and Estrogenic Disrupting Compounds on Fish Mineralized Tissues." *Marine Drugs* 12:4474–94.

Rao, Koppaka V., Sunil K. Chattopadhyay, and G. Chandrasekhara Reddy. 1990. "Flavonoids with Mosquito Larval Toxicity." *Journal of Agricultural and Food Chemistry* 38(6):1427–30.

Riveron, Jacob M., Cristina Yunta, Sulaiman S. Ibrahim, Rousseau Djouaka, Helen Irving, Benjamin D. Menze, Hanafy M. Ismail, Janet Hemingway, Hilary Ranson, Armando Albert, and Charles S. Wondji. 2014. "A Single Mutation in the GSTe2 Gene Allows Tracking of Metabolically Based Insecticide Resistance in a Major Malaria Vector." *Genome Biology* 15(2):1–20.

Saisawang, Chonticha, Jantana Wongsantichon, and Albert J. Ketterman. 2012. "A Preliminary Characterization of the Cytosolic Glutathione Transferase Proteome from Drosophila Melanogaster." *Biochemical Journal* 442(1):181–90.

Saito, Junki, Ryota Kimura, Yuya Kaieda, Ritsuo Nishida, and Hajime Ono. 2016. "Characterization of Candidate Intermediates in the Black Box of the Ecdysone Biosynthetic Pathway in Drosophila Melanogaster: Evaluation of Molting Activities on Ecdysteroid-Defective Larvae." *Journal of Insect Physiology* 93–94:94–104.

Scian, Michele, Isolde Le Trong, Aslam M. A. Mazari, Bengt Mannervik, William M. Atkins, and Ronald E. Stenkamp. 2015. "Comparison of Epsilon- and Delta-Class Glutathione S-Transferases: The Crystal Structures of the Glutathione S-Transferases DmGSTE6 and DmGSTE7 from Drosophila Melanogaster." *Acta Crystallographica Section D: Biological Crystallography* 71:2089–98.

Shelley, John C., Anuradha Cholleti, Leah L. Frye, Jeremy R. Greenwood, Mathew R. Timlin, and Makoto Uchimaya. 2007. "Epik: A Software Program for PKa Prediction and Protonation State Generation for Drug-like Molecules." *Journal of Computer-Aided Molecular Design* 21(12):681–91.

Shimada-Niwa, Yuko and Ryusuke Niwa. 2014. "Serotonergic Neurons Respond to Nutrients and Regulate the Timing of Steroid Hormone Biosynthesis in Drosophila." *Nature Communications* 5:5778.

Simons, P. C. and D. L. Vander Jagt. 1980. "Bilrubin Binding to Human Liver Ligandin (Glutathione S-Transferase)." *Journal of Biological Chemistry* 255(10):4740–44.

Sparks, Thomas C. and Ralf Nauen. 2015. "IRAC: Mode of Action Classification and Insecticide Resistance Management." *Pesticide Biochemistry and Physiology* 121:122–28.

Strode, Clare, Maria de Melo-Santos, Tereza Magalhães, Ana Araújo, and Contancia Ayres. 2012. "Expression Profile of Genes during Resistance Reversal in a Temephos Selected Strain of the Dengue Vector, Aedes Aegypti." *PLoS ONE* 7(8):1–8.

Tanaka, Shigenori, Yuji Mochizuki, Yuto Komeiji, Yoshio Okiyama, and Kaori Fukuzawa. 2014. "Electron-Correlated Fragment-Molecular-Orbital Calculations for Biomolecular and Nano Systems." *Physical Chemistry Chemical Physics*.

Tsukamoto, Takayuki, Koichiro Kato, Akifumi Kato, Tatsuya Nakano, Yuji Mochizuki, and Kaori Fukuzawa. 2015. "Implementation of Pair Interaction Energy DecompositionAnalysis and Its Applications to Protein-Ligand Systems." *Journal of Computer Chemistry, Japan*.

Udomsinprasert, Rungrutai, Saengtong Pongjaroenkit, Jantana Wongsantichon, Aaron J. Oakley, La Aied Prapanthadara, Matthew C. J. Wilce, and Albert J. Ketterman. 2005. "Identification, Characterization and Structure of a New Delta Class Glutathione Transferase Isoenzyme." *Biochemical Journal* 388(3):763–71.

Vagin, A. and A. Teplyakov. 1997. "*MOLREP* : An Automated Program for Molecular Replacement." *Journal of Applied Crystallography* 30(6):1022–25.

Voss, Neil R. and Mark Gerstein. 2010. "3V: Cavity, Channel and Cleft Volume Calculator and Extractor." *Nucleic Acids Research* 38(SUPPL. 2):555–62.

Warren, J. T., A. Petryk, G. Marques, M. Jarcho, J. P. Parvy, C. Dauphin-Villemant, M. B. O'Connor, and L. I. Gilbert. 2002. "Molecular and Biochemical Characterization of Two P450 Enzymes in the Ecdysteroidogenic Pathway of Drosophila Melanogaster." *Proceedings of the National Academy of Sciences* 99(17):11043–48.

Warren, James T., Anna Petryk, Guillermo Marqués, Jean Philippe Parvy, Tetsuro Shinoda, Kyo Itoyama, Jun Kobayashi, Michael Jarcho, Yutai Li, Michael B. O'Connor, Chantal Dauphin-Villemant, and Lawrence I. Gilbert. 2004. "Phantom Encodes the 25-Hydroxylase of Drosophila Melanogaster and Bombyx Mori: A P450 Enzyme Critical in Ecdysone Biosynthesis." *Insect Biochemistry and Molecular Biology* 34(9):991–1010.

Waterhouse, Andrew M., James B. Procter, David M. A. Martin, Michèle Clamp, and Geoffrey J. Barton. 2009. "Jalview Version 2-A Multiple Sequence Alignment Editor and Analysis Workbench." *Bioinformatics*.

Wieschaus, E. and C. Nüsslein-Volhard. 1986. "Looking at Embryos." Pp. 199–227 in *Drosophila: A Practical Approach*, edited by Roberts D. B. Oxford: IRL Press.

Williams, C. M. 1967. "Third-Generation Pesticides." *Sci. Am.* 217(1):13–17.

Wu, Baojian and Dong Dong. 2012. "Human Cytosolic Glutathione Transferases: Structure, Function, and Drug Discovery." *Trends in Pharmacological Sciences* 33(12):656–68.

Yamada, Y., N. Matsugaki, L. M. G. Chavas, M. Hiraki, N. Igarashi, and S. Wakatsuki. 2013. "Data Management System at the Photon Factory Macromolecular Crystallography Beamline." *Journal of Physics: Conference Series* 425(PART 1):0–4.

Yamanaka, Naoki, Kim F. Rewitz, and Michael B. O'Connor. 2012. "Ecdysone Control of Developmental Transitions: Lessons from Drosophila Research." *Annual Review of Entomology* 58:497–516.

Yoshiyama-Yanagawa, Takuji, Sora Enya, Yuko Shimada-Niwa, Shunsuke Yaguchi, Yoshikazu Haramoto, Takeshi Matsuya, Kensuke Shiomi, Yasunori Sasakura, Shuji Takahashi, Makoto Asashima, Hiroshi Kataoka, and Ryusuke Niwa. 2011. "The Conserved Rieske Oxygenase DAF-36/Neverland Is a Novel Cholesterol-Metabolizing Enzyme." *Journal of Biological Chemistry* 286(29):25756–62.

Yoshiyama, T. 2006. "Neverland Is an Evolutionally Conserved Rieske-Domain Protein That Is Essential for Ecdysone Synthesis and Insect Growth." *Development* 133(13):2565–74.

Yu, Quanyou, Cheng Lu, Bin Li, Shoumin Fang, Weidong Zuo, Fangyin Dai, Ze Zhang, and Zhonghuai Xiang. 2008. "Identification, Genomic Organization and Expression Pattern of Glutathione S-Transferase in the Silkworm, Bombyx Mori." *Insect Biochemistry and Molecular Biology* 38(12):1158–64.

Zhan, Shuai and Steven M. Reppert. 2013. "MonarchBase: The Monarch Butterfly Genome Database." *Nucleic Acids Research* 41(D1):758–63.